Kaminsky, F. V., Wirth (2011): Iron carbide inclusions in lower-mantle diamond from Juina, Brazil. - The Canadian Mineralogist, 49, 2, 555-572

DOI: 10.3749/canmin.49.2.555

IRON CARBIDE INCLUSIONS IN LOWER-MANTLE DIAMOND FROM JUINA, BRAZIL

Felix V. KAMINSKY*

KM Diamond Exploration Ltd., 2446 Shadbolt Lane, West Vancouver, British Columbia, V7S 3J1Canada

Richard WIRTH

Dept. Chemistry of the Earth, GeoForschungsZentrum Potsdam, D-14473Potsdam, Germany

Abstract

Iron carbides in association with native iron, graphite, and magnetite were identified in a diamond from the Juina area, Brazil, which contains a series of other, lower-mantle mineral inclusions. Among iron carbides, Fe_3C, Fe_2C ("chalypite"), and $Fe_{23}C_6$ (haxonite) are present; the two latter are identified in the terrestrial environment for the first time. Some of the analyzed iron carbide grains contain 7.3-9.1 at.% N and are, in fact, nitrocarbide. It is suggested, based on the high-pressure mineral paragenesis previously observed in the diamond and experimental data on the system Fe-C, that "chalypite" crystallized, within a pressure interval of 50-130 GPa, from an iron-carbon melt, rich in nitrogen. Following crystallization, iron carbides and native iron were partially oxidised to magnetite, and encapsulated in diamond along with other high-pressure minerals. The finds of various iron carbides, some of which are rich in nitrogen, in lower-mantle diamond confirm a significant role of carbides and nitrogen in the Earth's interior.

Keywords: diamond, iron carbide, nitrocarbide, cohenite, chalypite, haxonite, native iron, nitrogen, lower mantle, D" layer, outer core, TEM, Juina, Brazil.

Introduction

In recent decades, lower-mantle mineral inclusions in diamond from different areas were identified. Compositional features and associations of some grains of ferropericlase gave reasons to suggest their origin within the D" layer at the core – mantle boundary (Harte *et al*., 1999; Kaminsky *et al*., 2006). Recently one of diamond crystals from the Juina area in Brazil was found to contain carbonate and halide inclusions associated with wüstite + periclase association,

* *E-mail address*: felixvkaminsky@cs.com

presumably from the D" layer (Kaminsky *et al.*, 2009*a*). During the subsequent study of this diamond, presented here, another interesting association was identified: iron carbides + native iron + magnetite + graphite.

In this work, an occurrence of cohenite is described in addition to other iron carbides reported for the first time from the terrestrial environment. Here, we find that some of the analyzed iron carbide grains contain up to 9.1 at.% nitrogen and are, in fact, "nitrocarbide" that is also identified from the natural, terrestrial environment for the first time. We characterize these phases in this paper.

Background Information

Natural iron carbide samples were discovered and reported from the study of iron meteorites. Three iron carbides are known from meteorites to date: cohenite, chalypite, and haxonite. Cohenite, $(Fe,Ni,Co)_3C$, was described after its occurrence in the diamond-bearing iron meteorite Magura (Slovakia) in the 1840s; it was named after Professor E.M. Cohen and has the composition Fe_3C (Weinschenk, 1889). Since its discovery, cohenite has been identified in many other iron meteorites (Buchwald, 1975). Chalypite (as Fe_2C) was identified in 1854 by Forchhammer (1861) as a leading constituent of the Niakornak iron meteorite (from Greenland). The mineral was named by Shepard (1867) who, in his classification of meteorites, distinguished a special group of iron meteorites as "chalypitic", or "steel-like" (from the Greek word $\chi\alpha\lambda\upsilon\psi$ = steel); the principal mineral constituent of these meteorites was termed "chalypite". Chalypite has not subsequently been identified in any meteorite, following its initial discovery (probably because all iron carbides found in meteorites have been considered *a priori* to be cohenite; many of them were not analyzed). This absence provided grounds for Buchwald (1975) to consider the mineral as misinterpreted cohenite; later he offered to delete this mineral (Buchwald, 1977). This suggestion, in our opinion, was premature. Our chemical and structural data below confirm the existence of chalypite as a separate, natural mineral phase; and we use the original Shepard's (1876) name "chalypite", in this work, although it is not yet approved by the IMA. Haxonite $(Fe,Ni,Co)_{23}C_6$ was identified in the Toluca (Mexico) and Canyon Diablo (USA) iron meteorites by Scott (1971), as well as in several other iron meteorites (Buchwald, 1975). It occurs as a minor accessory in meteorites that also contain cohenite. Both cohenite and haxonite in meteorites are frequently found to have decomposed to "ferrite" (α-Fe) and graphite, reflecting thermodynamic instability for the former minerals at atmospheric pressure and temperature conditions (Buchwald, 1975). Cohenite was further reported in lunar rocks collected in almost all of the Apollo missions (Goldstein *et al.*, 1976) and in the lunar soil from various Luna missions (Barsukov & Tarasov, 1982).

In natural terrestrial environments, only one iron carbide, cohenite has been described until recently. It occurs usually in association with native iron as inclusions in diamond (Sharp, 1966; Bulanova & Zayakina, 1991; Jacob *et al.*, 2004; Jones *et al.*, 2008). In addition to its presence as inclusions within diamond from kimberlites, cohenite occurs in association with diamond,

wüstite, native iron and other minerals in ophiolitic chromitite from Luobasa, Tibet, along with another, recently discovered iron carbide, yarlongite $(Fe,Cr,Ni)_9C_4$ (Shi *et al.*, 2009). Besides diamond parageneses in kimberlite and ophiolite, cohenite + native iron + graphite associations are known from basaltic rocks found on Disko Island, Greenland (e.g., Goodrich and Bird, 1985; Ulff-Møller, 1985) and at the Bühl near Kassel in Germany (Irmer, 1920).

Besides these occurrences in the natural environment, cohenite as "cementite" and some other iron carbide varieties are well-known from and have been studied in metallurgy since the 1890s.

Sample and Analytical Techniques

The crystal selected for study, #8/1-3, is a dodecahedroid typical of the Juina area in Mato Grosso State, Brazil. Its dimensions are 5.2 × 4.9 × 3.8 mm. Optical microscopy reveals numerous inclusions of differing size and colour within this stone. The nitrogen concentration of diamond #8/103, detected with Fourier Transform Infrared Spectroscopy (FTIR), is 44 ppm and consists only of B-centres (N_B); i.e., this is a Type-IaB diamond (Kaminsky *et al*., 2009*a*). Such low concentration and high nitrogen aggregation ratios are characteristic for "deep" diamond (e.g., Hutchison *et al*., 1999; Kaminsky *et al.*, 2009*b*). Another interesting feature of this stone, like for most of the "deep" diamond crystals in the Juina area, is a high concentration of the hydrogen impurity centre identified at 3107 and 1405 cm^{-1} in the IR spectrum (Wirth *et al.*, 2009). Commonly, this centre is either absent or weakly expressed. In contrast to the majority of diamond deposits worldwide, almost all of the diamond crystals from the Juina pipes (80-89%) have noticeable (up to 4.2 cm^{-1}) levels of hydrogen C-H-centre (Kaminsky *et al.*, 2009*b*).

Diamond #8/1-3 was crushed, and individual diamond fragments were selected for focused ion beam (FIB) sample preparation. Only those inclusions in the diamond lying close to the surface (after crushing) were selected to be suitable for FIB-assisted transmission electron microscopy (TEM). Seven TEM foils were prepared from a single fragment (##2025, 2044, 2049, 2053, 2063, 2073, and 2106). Electron-transparent foils were milled by FIB techniques, applying a single-beam device (FEI FIB 200 TEM) operated at GFZ Potsdam (Ga-ion beam, 30 keV acceleration voltage). The foil thicknesses were found to vary from 100 to 150 nm. The electron transparent foils (typical dimensions: 15 × 10 × 0.15 μm) were cut normal to the diamond fragment surface. Details of the FIB sample preparation are given in Wirth (2004, 2009).

The foils were studied with TEM at the GFZ. A variety of TEM techniques, such as bright field – dark field imaging, high-angle annular dark-field imaging (HAADF), electron diffraction, electron-energy-loss spectroscopy (EELS), and analytical electron microscopy (AEM) were applied, utilising a TECNAI F20 XTWIN transmission electron microscope with a field emission gun as an electron source. This electron microscope is equipped with a Gatan Imaging Filter (GIF) Tridiem, an EDAX X-ray analyzer and a Fishione high-angle annular dark-field detector. Bright-field (BF), dark-field (DF) images, as well as high-resolution images, were invariably

acquired as energy-filtered images. For this purpose a 20 eV window was applied to the zero-loss peak. The quantification of Fe, C and N in the iron carbides was carried out from EEL spectra that contain both the C*K* edge and the Fe$L_{3,2}$ using the Digital Micrograph software package. The spectra were acquired in the diffraction mode with the electron beam focused; the beam size was approximately 2-5 nm. The total error of the relative quantification of Fe, C and N is less than 10%. The minimum detectable number of nitrogen atoms in a silicon matrix with EELS is in the range of 10^4 –10^5 atoms (Joy, 1986). The following parameters were applied during spectrum acquisition: spectrum dispersion - 0.3 eV/pixel; entrance aperture - 2 mm; camera length - 770 mm; convergence angle - 2.0 mrad; collection angle - 10.0 mrad; acquisition time - 1 second; model for calculating the cross section - Hartree Slater; back-ground model - power law. The trace-element composition in iron carbides in a diamond was measured with AEM and EELS. We used AEM (EDX) with an X-ray analyser with an ultra-thin window. The uncertainties for AEM measurements of Fe are approximately 3%; for Cr and Ni, they are approximately 10%. The X-ray intensity spectra were usually acquired in the scanning transmission mode (STEM) scanning the electron beam in a selected window approximately 20 × 20 nm in size (window analysis), thus reducing mass loss during the measurement significantly. It was impossible to use AEM for the carbon and nitrogen quantification because the X-ray fluorescence yield for C and N is very low, and no reliable k_{AB} factors[†] are available.

Results

Five of the seven studied foils (##2025, 2049, 2053, 2063, and 2073) contain polymineralic inclusions within the diamond, which are the parts of a single, flattened, graphite – iron carbide – native iron – magnetite inclusion. The inclusion is approximately 10 μm in two dimensions and up to 0.3 μm thick. Foils ##2025, 2049, and 2073 represent the major part of the inclusion, whereas foils ## 2053 and 2063 cut across it (#2053 in the central part and #2063 in the periphery of the inclusion). One of the foils (#2025) contains all four phases; the others represent the association iron carbide + graphite that comprises the bulk of the inclusion. The sixth foil (#2044) contains only graphite. Foil #2106 missed the inclusion.

All mineral phases were identified based on diffraction data (fast Fourier transforms, FFT), EEL spectra, and EDX spectra. Only in those cases where the calculated unit-cell parameters are in agreement with the observed data from the diffraction pattern was the phase identified unambiguously.

Foil #2025 contains a fragment of the inclusion, which has irregular shape and is approximately 2.5 × 4 μm in size. It is located within a diamond matrix with high density of dislocations. The inclusion is composed of four phases: iron carbide, native iron, magnetite, and graphite (Fig. 1). The magnetite grain, approximately 1.1 μm in size, is a polycrystalline

[†] The k_{AB} factor describes the relationship, in the Cliff-Lorimer equation, of the element concentrations in the sample with the measured intensities (Cliff & Lorimer, 1975). It is a constant at a given operating voltage.

aggregate with porosity, which was filled with fluid prior to the FIB milling. This magnetite grain is located near the foil surface. This particular fragment of diamond was at first laser-cut, and then crushed. The actual surface represents the interior of the original grain. As the extension of the inclusion above the present-day surface is unknown, we were unable to determine the precise location of this grain within the graphite – iron carbide – native iron – magnetite inclusion. The rim of the inclusion is composed of native iron, and the core of the inclusion is composed of iron carbide. Iron carbide is an aggregate of grains, 0.5-1 μm each, with high density of dislocations (Fig. 2). Some of the iron carbide grains (in the upper part of Fig. 1) display a zig-zag-like interface with graphite, caused, most likely, by the high density of dislocation in carbide. The iron carbide thus was corroded by graphite. In foil #2063, however, the reverse relationship can be seen, with the influence of iron carbide on graphite (see below) dominant. Moreover, some smaller grains of iron carbide are embedded in the graphite matrix.

Several EDX spectra were used in estimating the mineral compositions (Fig. 3). In some cases, they demonstrate the existence of impurities in the minerals, such as nitrogen in iron carbide (Fig. 3A) and in native iron (Fig. 3B).

According to electron-diffraction data, two phases were identified among iron carbide grains, Fe_3C and Fe_2C. Both iron carbide phases have an orthorhombic structure, but differ in their unit-cell dimensions: Fe_3C: $a_0 = 0.509$ nm, $b_0 = 0.6748$ nm, $c_0 = 0.4523$ nm (Wood *et al*., 2004); and Fe_2C: $a_0 = 0.4704$ nm, $b_0 = 0.4318$ nm, $c_0 = 0.2830$ nm (Hirotsu & Nagakura, 1972).

Fast Fourier transforms (FFT) diffractograms, acquired from high-resolution TEM images from the iron carbide phases, can be indexed as Fe_2C, shown as an example in Fig. 4A, and also as Fe_3C. From each diffractogram three vectors were measured and compared with the calculated lattice-spacings of Fe_3C and Fe_2C. The measured *d*-value of 0.434 nm fits d_{010} Fe_2C (0.4318 nm) very well but deviates from d_{001} Fe_3C (0.4523 nm). The measured *d*-value 0.232 nm matches d_{200} Fe_2C (0.2352 nm) and deviates from d_{210} Fe_3C (0.2381). The measured *d*-value of 0.204 nm is close to d_{210} Fe_2C (0.2065 nm) and d_{211} Fe_3C (0.2107 nm) within the measuring error. This diffractogram can be indexed as Fe_3C with the lattice planes (001), (211) and (210) with a zone axis of [1-20]. Alternatively, it can be indexed as Fe_2C with the lattice planes (010), (210) and (200) with a zone axis of [00-1].

The ultimate test for correct indexing of the diffraction pattern is the comparison of the measured angles between the vectors or lattice planes and the calculated angles between the corresponding lattice planes. In this particular diffraction pattern, we observe no substantial differences indexing the diffractogram as Fe_3C and Fe_2C. For example, in the case of the diffraction pattern shown in Fig. 4A it is obvious that indexing the diffractogram as Fe_2C the angles fit as well as for indexing it as Fe_3C. The calculated angle between (210) and (010) planes for Fe_2C is 61.4° (measured angle is 61.9°) and the calculated angle between (210) and (200) planes is 28.58° (measured angle is 27.8°). In comparison, the calculated angle between (211) and (001) planes for Fe_3C is 62.23°, whereas the observed angle is 61.9°. The calculated angle between (211) and (210) planes is 27.77° and the observed angle is 27.8°. In this case, the

electron diffraction data does not unambiguously allow the determination of one unique, and therefore correct iron carbide phase.

Qualitative EDX analysis of that iron carbide grain shows the presence of nitrogen in the iron carbide phase (Fig. 3A). In another iron carbide grain from foil #2053 we observed a iron carbide grain with the same diffraction pattern as mentioned above. However, in that grain we were able to measure the Fe/C ratio with EELS and thus to find a composition of Fe_2C. Additionally, this grain contained nitrogen, making it likely that the iron carbide grain in foil #2025 is also Fe_2C. Unfortunately, foil #2025 was not thin enough at that location to acquire a good quality EEL spectrum to quantify the Fe/C ratio. EDX analysis cannot be used to quantify nitrogen or carbon because there are no reliable k_{ab} factors available and because the fluorescence yield for these light elements is extremely low.

In *foil #2049*, a triangular inclusion, approximately 5 μm in size is observed. It is principally composed of polycrystalline graphite with finely dispersed (20-50 nm), irregularly shaped iron carbide grains (Fig. 5).

Much coarser grains of iron carbide (up to 2 μm in length) are visible along the interface with the host diamond. They form sharp, even iron carbide - diamond phase boundaries, and very irregular, corrosion-type ones with graphite. In this foil, iron carbide was determined as Fe_2C or Fe_3C in the diffraction patterns calculated from high-resolution images. The diffraction pattern with observed *d*-values 0.425, 0.234 and 0.202 nm can be indexed as Fe_3C ((001), (210) and (211) with the zone axis of [-120]) or Fe_2C ((200), (210), (010) with a zone axis of [001]). The measured angles between corresponding lattice planes are: 1) for Fe_2C: angle between (210):(010) is 60.8° (61.4° calc.) and between (210):(200) the angle is 28.8° (28.58° calc.); 2) for Fe_3C : angle between (211)/(210) = 28.8° (27.77° calc.) and between (211)/(001) = 62.04 (62.23° calc.). EELS measurements also could not be performed because the iron carbide grains were not thin enough to obtain reliable quantitative results.

In *foil #2053* a cross-cut of the inclusion, approximately 0.2-0.3 μm wide, runs through the entire foil (Figs. 6A, B). The diamond shows low density of dislocations in the vicinity of the plate. The inclusion consists of iron carbide crystals embedded in a graphite matrix. In the dark field image (Fig. 6B), a bright contrast of many of the iron carbide crystals indicates that they have the same crystallographic orientation. These grains thus were a single crystal that was subsequently replaced by graphite that disintegrated. Like in the case of foil #2049, iron carbide grains have sharp interfaces with diamond and invariably with rough and strongly curved interfaces with graphite; this is well demonstrated in Fig. 7 that also shows relics of iron carbide grains (less than 100 nm in size) embedded within the graphite matrix. Rarely, in the high-resolution electron microscopy (HREM) images, the iron carbide grains show moiré patterns, which is an interference pattern commonly observed if plate-like crystals with slightly different lattice spacings are stacked upon each other or if two crystals with the same lattice spacing are twisted with respect to one another.

The EELS and electron-diffraction data identified again (as in foil #2025) two structural and compositional varieties of iron carbide, Fe_3C and Fe_2C, based on lattice fringe spacing measured

from high-resolution images (FFT) (Figs. 4B, C). From each diffractogram, three vectors were measured and compared with calculated lattice-spacings of Fe_3C and Fe_2C.

Several diffraction patterns were indexed as Fe_3C. One of the diffraction patterns (Fig. 4B), as an example, was indexed as: (010) 0.675 nm (0.6748 nm calc.); (101) 0.337 nm (0.3381 nm calc.); (111) 0.299 nm (0.3023 nm calc.). The zone axis is [-101]. The angles between corresponding lattice planes are: (010):(111) = 63.8° obs. and 63.39° calc.; (101):(111) = 26.7° obs. and 26.61° calc. In this case, the *d*-value 0.675 nm, only matches the (010) plane of Fe_3C (Table 1). In addition, we were able to combine structural observations with chemical composition from EELS data for this iron carbide species. In the same grain, we measured Fe = 76.9 at.% and C = 23.1 at.% with a Fe/C ratio = 3.33 (Table 2, grain #11). However, other grains of the iron carbide phase could be indexed as Fe_2C. One of them, as an example (Fig. 4C), was indexed as: (010) 0.434 nm (0.4318 nm calc.); (200) 0.232 nm (0.2352 nm calc.); and (210) 0.204 nm (0.2065 nm calc.). The angles between corresponding lattice planes are as follows: (010):(210) = 61.8° obs. and 61.4° calc.; (200):(210) = 28.4° obs. and 28.58° calc. In addition, this diffraction pattern shows weak reflections between the (200) reflections that can be indexed as (100) planes, and others between (010) and (210) reflections that can be indexed as (110) planes. If we compare the observed lattice spacings of the weak reflections with the *d*-values of Fe_3C and Fe_2C, it becomes obvious that the *d*-values of Fe_2C match the observed values much better than of Fe_3C ones, and the 0.434 nm *d*-value does not match Fe_3C at all (Table 1). We conclude, therefore, that some of the iron carbide grains present in this sample are Fe_2C. This is also supported by the Fe/C ratio determined with EELS. The chemical composition of this grain (Table 2, grain #12) was different from the Fe_3C carbide: Fe = 62.8 at.%; C = 28.1 at.%; N = 9.1 at.%; Fe/C = 2.23 and Fe/(C+N) = 1.69. The presence of nitrogen in this grain is documented in the EEL spectrum.

In foil #2053, another carbide variety was identified. The diffraction pattern of that carbide phase is different from both Fe_3C and Fe_2C: (001) 0.447 nm; (100) 0.402 nm; and (101) 0.299 nm (Fig. 4D). As such, the peaks could be indexed based on the diffraction patterns of a synthetic alloy $\in$-$Fe_3(N_{0.80}C_{0.20})_{1.395}$ which has a Fe/(C+N) ratio 2.15, i.e., similar to the Fe_2C composition but with a C/(C+N) ratio of 0.20: (001) 0.4406 nm; (100) 0.4135 nm; and (101) 0.3015 nm (Leineweber *et al*., 2001). The C/N ratio in this synthetic alloy can vary because both carbon and nitrogen are located in the interstitial positions of the lattice (Leineweber *et al*., 2001). This compound, having a trigonal crystal structure, is called carbonitride and is of great importance to metallurgy.

Foil #2063 contains another, thin cross-cut (approximately 50 nm wide and 6 μm long) inclusion that is comprised mainly of iron carbide (predominant in this case) and some graphite. The iron carbide individual crystals are small (30-350 nm × 15-20 nm) platelets, oriented parallel to the borders of the inclusion (Fig. 8). At the curved tip of the iron carbide crystals, a thin layer of graphite (approximately 5-6 nm) coats the carbide tip following precisely its curvature (Fig. 9). The graphite seems to have crystallized after the formation of iron carbide and might represent in situ replacement of carbide.

Foil #2073 contains an equidimensional inclusion with a diameter of approximately 8.5 μm; it is composed mostly of graphite (Fig. 10). Irregularly shaped iron carbide grains, to 2 μm in size are developed within the graphite matrix and along its border with diamond (for example, in foils #2049 and #2053; Figs. 5-7). The carbide grains developed along the graphite - diamond border have, as usually, sharp, even boundaries with diamond and very irregular, strongly corroded ones with graphite.

In general, some general statements about the inclusion textures can be formulated as follows:

1. Iron carbides and graphite form the bulk of the inclusion, with graphite the predominant phase.
2. Iron carbides and native iron are polycrystalline aggregates composed of irregular, allotriomorphic grains, 0.5-1 μm in size, in some cases with high density of dislocations.
3. Iron carbides forms large (up to 2 μm) grains developed within a graphite matrix or along diamond interfaces, together with finely dispersed (< 50 nm), irregularly shaped grains within a graphite matrix.
4. Iron carbides and graphite are closely interrelated: in some cases, iron carbide influences the crystallization of graphite (e.g., foil #2063; Fig. 9); in other cases, large grains of iron carbide, developed along diamond grain-boundaries, have sharp boundaries with diamond, and very irregular, corrosion-type interface with graphite, indicating the replacement of iron carbide by graphite (Figs. 5-7, 10). In some areas, fragments of iron carbide adopt the initial orientation of the primary, large grain (foil #2053; Fig. 6B).
5. Magnetite is a minor mineral phase, and the only phase with porosity.

Characteristics of minerals

Native iron

Native iron, in foil #2025, was identified by FFT diffraction data (the lattice spacing 0.202 nm of the (101) reflections) and confirmed with the EDX spectrum (Fig. 3B). A minor nitrogen impurity was observed in the EDX spectrum; however, it cannot be quantified because there are no reliable k_{AB} data for nitrogen available. In another EDX spectrum, a minor admixture of Ni is also detected.

Graphite

Graphite, according to the high-resolution images, displays a characteristic lattice spacing of 0.335 nm for the (0002) lattice planes of graphite (foil #2063, Fig. 9). Other HREM images show that graphite is strongly deformed and does not appear as a single crystal. In general, the HREM images show that graphite is poorly crystallized. This is expressed in curved and bent (0002) lattice fringes and smeared out (0002) reflections in the diffraction patterns.

Magnetite

Magnetite, in foil #2025, forms a grain approximately 1.1 μm in size (Fig. 1). It was identified as iron oxide from EDX spectra (Fig. 3C) and confirmed as magnetite by diffraction data (FFT from high resolution images): 0.291 nm (022), 0.253 (311). The magnetite contains minor chromium (0.28 at.%; Table 3).

Iron carbides

Iron carbides comprise an important part of the inclusion and form an aggregate of euhedral grains, 0.5-1 μm in size. The diffraction data (Table 1) indicate that at least two varieties of iron carbide are present: cohenite and "chalypite". Iron carbide from foils #2025 and #2049 has evidence of both; however, the foils were not thin enough to obtain EELS measurements to discriminate between the two phases.

From foil #2053, fourteen grains were analyzed by means of EELS using the C*K* edge and the Fe$L_{3,2}$ edges. The chemical compositions of these grains, based on the EELS data, are presented in Table 2. The iron concentration varies from 62.2 to 79.9 at.%; the carbon from 20.1 to 37.8 at.%. This gives a wide range of Fe/C variations, from 1.65 to 3.98. Variations in concentrations of Fe and C, within the same grains (#9 and #10) are within the range of analytical error (± 10%), while differences in Fe/C values between different grains may be caused by differences in their structures. Grains #11 and #12 from Table 2, besides the EEL spectra, were analyzed structurally (analyses #3 and #7 in Table 1, respectively). The Fe/C values of these grains (3.33 for analysis #3, and 2.23 for analysis #7) correspond to Fe_3C (cohenite), and Fe_2C (chalypite), respectively.

The values of Fe/C differ from the stoichiometric ones not only because of the uncertainty of the measurement but, likely, because of the presence of other elements in the composition of the iron carbides. The major of those is nitrogen, which was identified in some EDX and EEL spectra. Fig. 11 represents an EEL spectrum of "chalypite" with a high concentration of nitrogen; in the analyzed cohenite, nitrogen was not observed. The quantification of nitrogen in the three "chalypite" grains (##12-14) gave its concentrations from 7.3 to 9.1 at.%.

Other admixtures in iron carbides are minor amounts of Cr (0-1.30 at.%) and Ni (0-0.50 at.%) (Table 3). This corresponds to analyses of other terrestrial cohenite, such as Ni = 0.6-3.1 wt.%, and Co = 0.3-0.6 wt.% (Goodrich & Bird, 1985; Ulff-Møller, 1985; Jacob *et al.*, 2004). Some lunar and meteoritic occurrences of cohenite, however, are richer in Ni (up to 4.1-7.0 wt.% in lunar samples, Goldstein *et al.*, 1976; and up to 2.3 wt.% in meteoritic samples, Buchwald, 1975).

The Fe/C values presented in Table 2 vary from grain to grain but remain almost constant within the same grain. Across one grain (#10), a profile was measured. Although Fe/C, in this profile, varies within a range of 0.31, it remains within the uncertainty of the measurement.

The variations in Fe/C from grain to grain are not gradual but have a discrete character. Considering the Fe/C variation for a single iron carbide variety of up to 0.7-0.8 (see chalypite Fe/(C+N) variations from 1.65 to 2.32 in grains ##12-14, Table 2), we grouped the fourteen analysed grains by their Fe/(C+N) values, to around 2, 3, and 4 (Fig. 12). Most grains are, therefore, "chalypite" with Fe/C varying from 1.65 to 2.32 at.% (nine grains, or 64.1%); 21.4% are cohenite with Fe/C from 3.02 to 3.39. Two grains have Fe/C from 3.59 to 3.98 and may be haxonite $(Fe,Ni,Co)_{23}C_6$, for which the theoretical Fe/C ratio is 3.83 (Scott, 1971).

Discussion

Iron carbide paragenesis

The first discovery of cohenite as an inclusion in diamond and in that case in association with troilite was made in a monocrystalline diamond from the South African Jagersfontein pipe by Sharp (1966). Later Bulanova & Zayakina (1991) found cohenite included in monocrystalline diamond from the Siberian XXIII Party Meeting pipe in association with native iron, graphite and silicate. In that inclusion, an aggregate of cohenite and native iron surrounds graphite, which comprises the bulk of the inclusion, - exactly like in our sample. It was concluded that the observed association was formed within the diamond stability field. Following these discoveries in monocrystalline diamond, cohenite has also been identified in a polymineralic diamond aggregate (bort) from the Venetia mine, in the Republic of South Africa where cohenite is associated with native iron, troilite and graphite. Jacob *et al.* (2004) concluded that the cohenite formed at the base of the subcratonic lithosphere from a C-H-O fluid, and that native iron was formed as a result of decomposition of cohenite. However, this model cannot be applied to our case because the Venetia cohenite is encapsulated within an eclogitic garnet, and the host diamond has an "eclogitic" signature with a light carbon isotopic composition ($\delta^{13}C$ = -13.69 ‰ PDB); the diamond aggregate, most likely, was formed during the course of the subduction of a lithospheric plate. Recently, cohenite has been reported in a series of diamond crystals from the Jagersfontein pipe, South Africa, where it associates with other, Fe-Cr (Cr up to 15 wt.%) and Fe-Ni (Ni up to 9.3 wt.%) carbides. According to preliminary data, X-ray diffraction patterns of these carbides do not confirm the presence of cohenite, and their metal/carbon (M/C) ratio varies from 3.14 to 4.31 (Jones *et al.*, 2008). In diamond from Siberia and Venetia, cohenite is associated with native iron and graphite.

Native iron was initially discovered in diamond from Siberian kimberlitic pipes Mir, Aikhal, and Udachnaya, where it is associated with silicates and sulphides (Sobolev *et al.*, 1981). Later native iron in Siberian diamond was confirmed by Garanin & Kudryavtseva (1990). In another Siberian pipe, XXIII Party Congress, native iron was identified in a touching association with cohenite and graphite (Bulanova & Zayakina, 1991). Native iron was found as well in diamonds from the Sloan pipe, USA (Meyer & McCallum, 1986); from Mwadui kimberlite, Tanzania, in association with primary wüstite and magnetite (Stachel *et al.*, 1998); from placer deposits in

Myanmar (Win *et al.*, 2001); and from the pipe Pandrea-2, Brazil (Kaminsky *et al.*, 2009*b*). All these finds are primary, syngenetic (or formed prior) to diamond inclusions.

Magnetite is observed as an inclusion in diamond more frequently. After an early discussion concerning its origin in diamond, the research of Harris (1968) and Meyer & Tsai (1976) proved that magnetite may be a primary phase in diamond. Primary magnetite is found as inclusions in diamond from Arkansas, USA (Pantaleo *et al.*, 1979), from Pipe 50, Liaoning, China (Gorshkov *et al.*, 1997), from Guaniamo, Venezuela (with high, 15.2 wt.% TiO_2; Sobolev *et al.*, 1998), from the Dokolwayo kimberlite, Swaziland, Southern Africa (Daniels & Gurney, 1999), and from placer deposits in the Ukraine (Kvasnytsya & Wirth, 2009). In all these finds, magnetite in diamond usually associates with silicates and various oxides, but never with carbide. In one of the Siberian inclusions in diamond, magnetite forms a rim on native iron (Sobolev *et al.*, 1981). In the studied by us sample from Juina, magnetite develops after a native iron-carbide aggregate.

Our polymineralic inclusion is very unusual. The iron carbide present is not a single species, cohenite, Fe_3C; two other iron carbides also are present, "chalypite" and potentially haxonite that has never before been observed in a terrestrial sample. For the first time, all three iron carbides are found to coexist, forming a series "chalypite" – cohenite – haxonite.

Such series of Fe, Co, Ni, Cr, and Mn carbides are well studied in technical applications. They belong to so-called intermediate transition-metal carbides, which share features with both the interstitial and the salt-like carbides. Like the interstitial carbides, iron carbides are metal-like compounds that have no ion connection in their crystal lattice; in their structures, carbon atoms occupy interstices between closely packed metal atoms. Different positions of metal atoms, in a crystal lattice, leads to multiple stoichiometries, such as $M_{23}C_6$, M_3C, M_7C_3, M_3C_2, M_4C_3, MC, MC_2 with variable (but fixed for each stoichiometry) M/C ratios (e.g., Kosolapova, 1971; Cottrell, 1995).

Chemical composition of "chalypite"

The exact chemical formula of "chalypite" is still unclear. In the first analyses from the Niakornak meteorite, carbon content was documented at between 7.23 and 11.06 wt.%, "which would indicate the formula of Fe_2C for this species" (Shepard, 1867, p. 28). In all later references (e.g., Weinschenk, 1889; Strunz, 1978), this mineral has a quoted formula of Fe_2C, although Shepard himself, considering uncertainty in the carbon determination, indicated "chalypite" as Fe*C*. Indeed, in those first analyses, the F/C value varies from 1.74 to 2.75.

Our analyses of "chalypite" have a similar range in F/C, 1.65-2.32 for nine grains (13 analyses, Table 2). Considering them as a single group, the average composition may be approximated as Fe_2C. However, in metallurgy, iron carbide Fe_7C_3 is a stable phase (with an average Fe/C value 2.33), but Fe_2C is not known. Fe_7C_3 is considered as an isomorph with Cr_7C_3, Ru_7B_3 and other substances (Herbstein and Snyman, 1964). Several polytypes and two structures of Fe_7C_3 (orthorhombic and hexagonal) are known now (Fang *et al*., 2009 and references therein). The compound Fe_7C_3 crystallizes at higher pressures than "cementite" (cohenite) Fe_3C

(Tsuzuki *et al.*, 1984). Based on the experimental data, an association $(Fe,Ni)_7C_3$ + diamond is considered as the major reservoir of carbon in deep Earth (Dasgupta & Hirshmann, 2010).

We suggest that the composition of meteoritic "chalypite" might also be Fe_7C_3, and may be applied to the terrestrial "chalypite" as well. During the course of decompression, Fe_7C_3 decomposes into Fe_3C + carbon (Tsuzuki *et al.*, 1984), and could explain why we have two carbide phases in our samples: "chalypite" is the relict phase, and cohenite is the decomposition one; and why graphite predominates in the association. Graphite comprises ~81-84 vol.% of the system (83.7% in foil 2049, Fig. 5; and 81.7% in foil #2073, Fig. 10). In addition, such a mechanism explains the secondary character of graphite; it represents a corrosion-type replacement of iron carbide (Figs. 5-7, 10).

Thermodynamic conditions of iron carbide and graphite formation and the history of the association

The system Fe-C at 1 atm pressure has a eutectic at ~1150 ^{o}C and *ca.* 4 wt.% C (Okamoto, 1990). Under pressures of 5-10 GPa, the eutectic point moves toward a greater carbon concentration (*ca*. 4.2-4.5 wt.%) at higher temperatures: 1250 ^{o}C at 5 GPa (Chabot *et al.*, 2008), 1370 ^{o}C at 5.6 GPa (Strong and Tuft, 1973), and 1420 ^{o}C at 10 GPa (Lord *et al.*, 2009). During eutectic growth, grain boundaries of "cementite" in steels are commonly allotriomorphic, as is evident in our sample (e.g., Aaronson, 1962). At pressures in excess of 10 GPa, there is a decrease in the carbon content, as the eutectic falls rapidly (Lord *et al.*, 2009); at pressures found in the Earth's core (i.e., up to 136 GPa), the carbon content, at the eutectic, is expected, therefore, to be very low (Wood, 1993). In contrast, the experimental work of Nakajima *et al.* (2009) provided different values for the position of the eutectic point, and it was found that Fe_7C_3, not Fe_3C could, in their opinion, be the primary crystallizing carbide phase in the Earth's core.

In the system Fe-C, cohenite-"cementite", Fe_3C, is stable at pressures of less than 5-6 GPa. At higher pressures, Fe_7C_3 becomes the stable species (Shterenberg *et al*., 1975; Tsuzuki *et al.*, 1984; Nakajima *et al.* 2009); at 50 GPa both Fe_3C and Fe_7C_3 are stable and coexist in subsolidus until ~120 GPa, corresponding to depths of ~3,400 km (i.e., within the outer core), where cohenite fully disappears, and only Fe_7C remains stable in association with diamond in both the liquidus and subsolidus associations (Lord *et al.*, 2009) (Fig. 13). Accordingly, one should expect that, under outer-core to lower-mantle conditions, Fe_7C_3 (exclusively or predominantly) should crystallize from an iron-carbon liquid. It is interesting that in the Fe-C system, under such extreme *P-T* conditions (starting from ~3,700 km depth in the outer core) diamond crystallizes first and can associate, in the subsolidus, with Fe_7C_3 and with cohenite Fe_3C, if the carbon concentration is sufficient (Fig. 13). Also, the initial system represents a local enrichment with carbon where graphite comprises ~81-84 vol.% of the system. Taking into account that in carbides, carbon comprises 20.1-37.8 at.% (Table 2), this gives an approximate carbon

concentration, in the observed system, at ~86-90 at.%, figure more than sufficient to make the system oversaturated with respect to carbon.

Which carbon phase, diamond or graphite crystallizes together with Fe_7C_3, depends on the temperature of crystallization. At higher temperatures graphite is stable, at lower temperatures diamond crystallizes, and closer to the eutectic point, Fe_7C_3, and then Fe_3C crystallizes (Shterenberg *et al*., 1975; Lord *et al.*, 2009). In addition to the temperature, the concentration of nitrogen plays important role in crystallization of different carbon phases (diamond and graphite). Recent experiments performed by Palyanov *et al.* (2010) in a Fe-Ni-C system within the diamond stability field demonstrated that, with increasing concentration of nitrogen, the growth of a single crystal diamond is followed by formation of block twinned crystals, increasing of density of dislocations (like in our sample) and then by crystallization of metastable graphite. This explains the existence of the association: graphite + diamond + "chalypite" + cohenite + native iron (some of these phases may be metastable); the latter exists, in metallurgical solidus systems, as austenite (γ-Fe). Magnetite, in the observed natural association, is an additional, disequilibrium, secondary phase formed as a result of partial oxidation of primary phases, iron carbide and native iron.

These experimental data, combined with the presence, in the Juina diamond investigated, of stable, lower-mantle mineral phases, that includes the association: wüstite + periclase from the D" layer at the core-mantle boundary (Kaminsky *et al.*, 2009*a*), confirm that an association of diamond + "chalypite" + graphite may crystallize from an iron-carbon liquid (locally enriched in carbon) either in the region of the uppermost stratified layer within the outer core or at the D" layer, along with the association wüstite + periclase.

The presence of native iron and graphite, in the iron carbide associations studied, indicates that the oxygen fugacity for this association was lower than the iron-wüstite oxygen buffer (*ca*. -9.5 to -10.5 log fO_2; Taylor, 1990; Fedorov *et al.*, 2002), and possibly as low as *ca*. -14 log fO_2, as was estimated by Solovova *et al.* (2002) for the association: native iron + cohenite in basalt from Disko Island, Greenland. Such highly reduced conditions might have occurred early in the history of Earth; for example, according to the model of the Earth's core growth by Galimov (2005), such conditions prevailed during only the first 100 million years of the Earth's development.

Subsequently, the oxygen fugacity became higher, and oxidation of native iron and iron carbide started with the formation of magnetite. However, because this process was not developed until the total oxidation of native iron and iron carbides, the existing association in diamond, which trapped the partially oxidised association, remained in disequilibrium. The analogous disequilibrium association: native Fe + magnetite has been observed in natural environment earlier, in one of the primary, rosette-like inclusions in diamond from the Mir pipe, Siberia (Sobolev *et al.*, 1981).

During the course of partial (and local) oxidation, nitrogen, which initially was incorporated in iron carbide ("nitrocarbide"), was unable to remain in magnetite; it was released, resulting in

the formation of porous magnetite. In other mineral phases (carbides/nitrocarbides and native iron) nitrogen remained as part of their composition.

Nitrogen in "chalypite"

A noticeable compositional feature of "chalypite" is a high concentration of nitrogen, identified in some grains. The admixture of nitrogen in iron carbide was identified via EDX spectra (Fig. 3A). Moreover, this high concentration of nitrogen was quantified by means of EELS spectra, such that in some "chalypite" grains, the 7.3-9.1 at.% provides a C/(C+N) anion ratio within a range of 0.73-0.81 (Fig. 11; Table 2), and allows the consideration of this mineral as nitrocarbide. One of the grains from foil #2053, according to its diffraction patterns (Fig. 4D; Table 1, anal. #10), is carbonitride with an approximate ratio value C/(C+N) ~ 0.20 (i.e., an extreme predominance of nitrogen over carbon); its Fe/(C+N) ratio is 2.17 which is close to stoichiometric "chalypite" (2.33, as we suggest).

To our knowledge, nitrocarbides and carbonitrides are not found under natural terrestrial conditions. However, nitrides (osbornite TiN and BN) are known in chromitites from the Luobasa, Tibet ophiolites, where they associate with diamond (Dobrzhinetskaya *et al.*, 2009).

In our sample, not only "chalypite" but native iron as well has a noticeable nitrogen impurity (Fig. 3B). The entire Fe-C system thus was enriched in nitrogen, and that nitrogen may play important role in the deep mantle and the D" layer. Not occasionally, high concentrations of nitrogen were identified only in the composition of "chalypite", which is the deepest mineral phase in the Fe-C system. The deeper is the origin of the phase (association), the more it is enriched in nitrogen.

Role of iron carbides and nitrogen in the Earth's interior

According to geophysical and experimental data, iron carbides play, along with iron, a significant role in the composition of the Earth's interior. The liquid outer core is ~3-8% less dense than molten iron. Moreover, compressional sound waves travel ~3% faster in this material as opposed to through molten iron, under comparable conditions. Hence lighter elements, such as H, C, O, among others, have been considered as most probable additional core components (e.g., Wood, 1993 and references therein). High-pressure experiments and their extrapolations allowed Scott *et al.* (2001) to conclude that iron carbide fulfill the density and elastic criteria necessary to be present in the Earth's outer core, and that carbon (along with hydrogen and sulfur) could be a major alloying component in the Earth's core. These conclusions can be applied to the inner core as well, where the density deficit is lower but still significant (~2.5-9%). Iron carbide in the inner core would explain both the observed seismic anisotropy and the density of the inner core, which is lower than pure iron under corresponding pressure and temperature conditions (Gao *et al.*, 2009). According to the data on sound velocity for iron carbide at high pressures, a reduced carbon content in the inner core (corresponding to ~1 wt.% of carbon) could reasonably explain

density and velocity differences between measurements made on pure iron and the seismic models (Fiquet *et al.*, 2009).

The Earth's core is a major reservoir of nitrogen. Nitrogen concentration in the core is ~0.5 wt.% (Sugiura, 1998), and its content for the core is estimated at ~1×10^{24} g, which is several magnitudes higher than the total N budget in other parts of the Earth (Miyazaki *et al.*, 2004). The solubility of N in molten iron was reported to be ~0.05 wt.% at 1600 ^{o}C; and it rapidly increases with decreasing fO_2 (Miyazaki *et al.*, 2004). According to high-pressure experiments, the most probable concentrators of nitrogen are iron nitrides; the most stable of them is Fe_7N_3, which was synthesised at 51 GPa and is stable up to 168 GPa. For this reason, Fe_7N_3 is suggested to be a part of the inner core (Adler and Williams, 2005).

Our data correspond to these conclusions and experiments. The system Fe-C-N, in various combinations, is the most likely model of the Earth's core and worth studying experimentally in more detail.

Conclusions

1. A series of iron carbides, "chalypite" – cohenite – haxonite is present as a composite inclusion in diamond. This series is analogous to industrial iron carbides having the same compositions.
2. "Chalypite" is confirmed as a natural compound both structurally and chemically. Some "chalypite" grains are greatly enriched in nitrogen (7.3-9.1 at.%) and are, therefore, a nitrocarbide.
3. The series "chalypite" – cohenite – haxonite, along with native iron, is associated with lower-mantle minerals, included in diamond. Some of the mineral inclusions (wüstite + periclase) were formed, most likely, within the D" layer, at the core-mantle boundary.
4. We suggest, on the basis of high-pressure mineral paragenesis and experimental data on the system Fe-C, that "chalypite" crystallized within a pressure interval of 50-130 GPa from an iron-carbon melt that was rich in nitrogen which, possibly, had its source in the outer core or within the D" layer.
5. Following crystallization, iron carbides and native iron were partially (locally) oxidised to magnetite, which released nitrogen to form pores in magnetite. The resulting, disequilibrium association was encapsulated in diamond along with a variety of other high-pressure minerals.
6. The transportation of the resulting polyphase inclusion in diamond was, possibly, complex. The diamond may have been involved into the mantle convection process. At the final stage it was delivered to the Earth's surface as a result of kimberlitic eruption.

Acknowledgements

The authors thank A. Schreiber for milling TEM foils for use in the FIB technique, two anonymous reviewers and Prof. I. Coulson whose critical notes helped to improve the manuscript.

References

Aaronson, H.I. (1962): The proeutectoid ferrite and the proeutectoid cementite reactions. *In: Decomposition of Austenite by Diffusional Processes* (V. Zackay and H.I. Aaronson, editors). Interscience, New York, pp. 387-546.

Adler, J.F. & Williams, Q. (2005): A high-pressure X-ray diffraction studies of iron nitrides: Implications for Earth's core. *J. Geophys. Res.* **110**, B011203, 11 pp.

Barsukov, V.L. & Tarasov, L.S. (1982): Moon rock mineralogy. *Int. Geol. Rev.* **26**, 238-248.

Buchwald, V.F. (1975): *Handbook of iron meteorites, their history, distribution, composition, and structure.* Volume 1. Tempe & Berkeley, Center for Meteorite Studies, and University of California Press, 243 pp.

Buchwald, V.F. (1977): Mineralogy of Iron Meteorites. *Phil. Trans. Series A, Mathematical and Physical Sciences* **286**, 453-491.

Bulanova, G.P. & Zayakina, N.V. (1991): Graphite – iron – cohenite assemblage in the central zone of diamond from 23rd Party Congress kimberlite. *Dokl. Akad. Nauk SSSR* **317**, 706–709 (in Russ.).

Bundy, F.R. (1963): Direct conversion of graphite to diamond in static pressure apparatus. *J. Chem. Phys* **38**, 631-643.

Chabot, N.L., Campbell, A.J., McDonough, W.F., Draper, D.S., Agee, C.B., Humayun, M., Watson, H.C., Cottrell, E. & Saslow, S.A. (2008): The Fe–C system at 5 GPa and implications for Earth's core. *Geochim. Cosmochim. Acta* **72**, 4146–4158.

Cliff, G. & Lorimer, G.W. (1975): The quantitative analysis of thin specimen. *J. Microscopy* **103**, 203-207.

Cottrell, A.H. (1995): *Chemical bonding in transition metal carbides*. Institute of Metals, London, 97 pp.

Daniels, L.R.M. & Gurney, J. (1999): Diamond Inclusions from the Dokolwayo Kimberlite, Swaziland. *In:* Gurney, J.J., Gurney, J.L., Pascoe, M.D. and Richardson, S.H. (eds), Proceedings of the VII International Kimberlites Conference, Cape Town, South Africa, Vol. 1. Red Roof Design, Cape Town, pp. 134-142.

Dasgupta, R. & Hirschmann, M.M. (2010): The deep carbon cycle and melting in Earth's interior. *Earth Planet. Sci. Lett.* **298**, 1-13.

Dobrzhinetskaya, L.F., Wirth, R., Yang, J., Hutcheon, I.D., Weber, P.K. & Green, H.W., II. (2009): High-pressure highly reduced nitrides and oxides from chromitite of a Tibetan ophiolite. *Proc. Nat. Academy Sciences* **106**, 19233-19238.

Fang, C.M., van Huis, M.A. & Zandbergen, H.W. (2009): Structural, electronic, and magnetic properties of iron carbide Fe_7C_3 phases from first-principles theory. *Physical Review B* **80**, 224108, 9 pp.

Fedorov, I.I., Chepurov, A.A. & Dereppe, J.M. (2002): Redox conditions of metal-carbon melts and natural diamond genesis. *Geochem. J.* **36**, 247-253.

Fiquet, G., Badro, J., Gregoryanz, E., Fei, Y. & Occelli, F. (2009): Sound velocity in iron carbide (Fe_3C) at high pressure: Implications for the carbon content of the Earth's inner core. *Physics Earth Planet. Inter.* **172**, 125–129.

Forchhammer, J.G. (1861): Fortegnelse over de i Universitetets Mineralsampling opbevarede Meteoriter. *Oversigt over det Kongelige Danske Videnskabernes Selskabs Forhandlinger, Copenhagen*, June, 225-229.

Fruchart, D., Chaudouet, P., Fruchart, R., Rouaul, A. & Senateur, J.P. (1984): Etudes structurales de composés de type cémentite: Effet de l`hydrogène sur Fe_3C suivi par diffraction neutronique. *J. Solid State Chemistry* **51**, 246-252.

Galimov, E.M. (2005): Redox evolution of the Earth caused by a multi-stage formation of its core. *Earth Planet. Sci. Lett.* **233**, 263– 276.

Gao, L., Chen, B., Lerche, M., Alp, E.E., Sturhahn, W., Zhao, J., Yavaş, H. & Li, J. (2009): Sound velocities of compressed Fe_3C from simultaneous synchrotron X-ray diffraction and nuclear resonant scattering measurements. *J. Synchrotron Radiation* **16**, 9 pp. doi: 10.1107/S0909049509033731.

Garanin, V.K. & Kudryavtseva, G.P. (1990): Morphology, physical properties and paragenesis of inclusion-bearing diamonds from Yakutian kimberlites. *Lithos* **25**, 211-217.

Goldstein, G.I., Hewins, R.H. & Romig, A.D., Jr. (1976): Carbides in Lunar soils and rocks. *Abstracts of the Lunar and Planetary Science Conference* **7**, 310-312.

Goodrich C.A. & Bird J.M. (1985): Formation of iron-carbon alloys in basaltic magma at Uivfaq, Disko Island; the role of carbon in mafic magmas. *J. Geology* **93**, 475–492.

Gorshkov, A.I., Bao, Y.N., Bershov, L.V., Ryabchikov, I.D., Sivtsov, A.V. & Lapina, M.I. (1997): Inclusions of native metals and other minerals in diamond from kimberlite Pipe 50, Liaoning, China. *Geochem. Int.* **35**, 695-703.

Harris, J.W. (1968): The recognition of diamond inclusions. Part 1. Syngenetic mineral inclusions. *Ind. Diamond Rev.*, 28, 402-410.

Harte, B., Harris, J.W., Hutchison, M.T., Watt, G.R. & Wilding, M.C. (1999): Lower mantle mineral associations in diamond crystals from Sao Luiz, Brazil. *In*: Mantle Petrology: Field Observations and High Pressure Experimentation: A Tribute to Francis R. (Joe) Boyd (Yingwei Fei, C.M. Bertka & B.O. Mysen, eds.). The Geochemical Society Special Publication No. 6, pp. 125-153.

Herbstein, H. & Snyman, J.A. (1964): Identification of Eckstrom-Adcock iron carbide as Fe_7C_3. *Inorganic Chemistry* **3**, 894-896.

Hirotsu, Y. & Nagakura, S. (1972): Crystal structure and morphology of the carbide precipitated from martensitic high carbon steel during the first stage of tempering. *Acta Metallurgica* **20**, 645-655.

Hutchison, M.T., Cartigny, P. & Harris, J.W. (1999): Carbon and nitrogen compositions and physical characteristics of transition zone and lower mantle diamonds from Sao Luiz, Brazil. *In*: Gurney, J.J., Gurney, J.L., Pascoe, M.D. and Richardson, S.H. (eds), Proceedings of the VIIth International Kimberlite Conference, vol. 1, Red Roof Design, Cape Town, pp. 372-382.

Irmer, W. (1920): Der Basalt des Bühls bei Kassel und seine Einschlüsse von Magnetit, Magnetkies und gediegen Eisen. *Abhandlungen der Senckenbergischen Naturforschenden Gesellschaft* **13**, 91–108.

Jacob, D.E., Kronz, A. & Viljoen, K.S. (2004): Cohenite, native iron and troilite inclusions in garnets from polycrystalline diamond aggregates. *Contrib. Mineral. Petrol.* **146**, 566–576.

Jones, A.P., Dobson, D., Wood, I., Beard, A.D., Verchovsky, A. & Milledge, H.J. (2008): Iron carbide and metallic inclusions in diamonds from Jagersfontein. *9th International Kimberlite Conference*, Extended Abstract No. 9IKC-A-00360, 3 pp.

Joy, D.C. (1986): Quantitative microanalysis using EELS. *In: Principles of analytical electron microscopy* (D.C. Joy, A.D. Romig, Jr. & J.I. Goldstein, editors), Plenum Press, New York, pp. 277-298.

Kaminsky, F.V., Zakharchenko, O.D., Khachatryan, G.K., Griffin, W.L. & Channer, D.M.DeR. (2006): Diamond from the Los Coquitos Area, Bolivar State, Venezuela. *Can. Mineral.* **44**, 323-340.

Kaminsky, F., Wirth, R., Matsyuk, S., Schreiber, A. & Thomas, R. (2009*a*): Nyerereite and nahcolite inclusions in diamond: evidence for lower-mantle carbonatitic magmas. *Mineral. Mag.* **73**, 797-816.

Kaminsky, F.V., Khachatryan, G.K., Andreazza, P., Araujo, D. & Griffin, W.L. (2009*b*): Super-deep diamonds from kimberlites in the Juina area, Mato Grosso State, Brazil. *Lithos* **112S**, 833-842.

Kosolapova, T.Ya. (1971): *Carbides: properties, production, and applications*. Plenum Press, New York-London, 298 pp.

Kvasnytsya, V.N. & Wirth, R. (2009): Nanoinclusions in microdiamonds from Neogenic sands of Ukraine (Samotkan' placer): a TEM study. *Lithos* **113**, 454-464.

Leineweber, A., Jacobs, H., Hüning, F., Lueken, H. & Kockelmann, W. (2001): Nitrogen ordering and ferromagnetic properties of $\in$-Fe_3N_{1+x} ($0.10 \leq x \leq 0.39$) and $\in$-$Fe_3(N_{0.80}C_{0.20})_{1.38}$. *J. Alloys Compounds* **316**, 21–38.

Lord, O.T., Walter, M.J., Dasgupta, R., Walker, D. & Clark, S.M. (2009): Melting in the Fe–C system to 70 GPa. *Earth Planet. Sci. Lett.* **284**, 157–167.

Meyer, H.O.A. & McCallum, M.E. (1986): Mineral inclusions in diamonds from the Sloan kimberlites, Colorado. *J. Geology* **94**, 600-612.

Meyer, H.O.A. & Tsai, H.-M. (1976): The nature and significance of mineral inclusions in natural diamond: a review. *Minerals Science Engineering* **8**, 242-261.

Miyazaki, A., Hiyagon, H., Sugiura, N., Hirose, K. & Takahasi, E. (2004): Solubilities of nitrogen and noble gases in silicate melts under various oxygen fugacities: Implications for the origin and degassing history of nitrogen and noble gases in the Earth. *Geochimica et Cosmochimica Acta* **68**, 387–401.

Nakajima, Y., Takahashi, E., Suzuki, T. & Funakoshi, K.-i. (2009): "Carbon in the core" revisited. *Physics Earth Planet. Inter.* **174**, 202–211.

Okamoto H. (1990): C–Fe (Carbon–Iron). *In: Binary Alloy Phase Diagrams*, Second edition, vol. 1 (T.B. Massalski, editor), ASM International, pp. 842-848.

Palyanov, Y.N., Borzdov, Y.M., Khokhryakov, A.F., Kupriyanov, I.N. & Sokol, A.G. (2010): Effect of nitrogen impurity on diamond crystal growth processes. *Crystal Growth Design* **10**, 3169-3175.

Pantaleo, N.S., Newton, M.G., Gogineni, S.V., Melton, C.E. & Giardini, A.A. (1979): Mineral inclusions in four Arkansas diamonds: their nature and significance. *Amer. Mineral.* **64**, 1059-1062.

Scott, E.R.D. (1971): New carbide $(Fe,Ni)_{23}C_6$, found in meteorites. *Nature Physical Sciences* **229**, 61-62.

Scott, H.P., Williams, Q. & Knittie, E. (2001): Stability and equation of state of Fe_3C to 73 GPa: Implications for carbon in the Earth's core. *Geophysical Res. Lett.* **28**, 1875-1878.

Sharp, W.E. (1966): Pyrrhotite: a common inclusion in South African diamonds. *Nature* **211**, 402-403.

Shepard, C.U. (1867): New classification of meteorites with an enumeration of meteoric species. *Amer. J. Science and Arts, Second Series* **43**, 22-28.

Shi, N., Bai, W., Li, G., Xiong, M., Fang, Q., Yang, J., Ma, Z. & Rong, H. (2009): Yarlongite: A new metallic carbide mineral. *Acta Geol. Sinica* **83**, 52-56.

Shterenberg, L.E., Slesarev, V.N., Korsunskaya, I.A. & Kamenetskaya, D.S. (1975): The experimental study of the interaction between the melt, carbides and diamond in the iron - carbon system at high pressures. *High Temperatures - High Pressures* **7**, 517 -522.

Sobolev, N.V., Efimova, E.S. & Pospelova, L.N. (1981): Native iron in Yakutian diamonds and its mineral assemblage. *Geologia i Geofizika (Russ. Geol. Geophys.)*, No. 12, 25–28 (in Russ.).

Sobolev, N.V., Yefimova, E.S., Channer, D.M., Anderson, P.F.N. & Barron, K.M. (1998): Unusual upper mantle beneath Guaniamo, Guyana shield, Venezuela: Evidence from diamond inclusions. *Geology* **26**, 971-974.

Solovova, I.P., Ryabchikov , I.D., Girnis, A.V., Pedersen, A. & Hansteen, T. (2002): Reduced magmatic fluids in basalt from the island of Disko, central West Greenland. *Chem. Geol.* **183**, 365–371.

Stachel T., Harris J.W. & Brey G.P. (1998): Rare and unusual mineral inclusions in diamonds from Mwadui, Tanzania. *Contrib. Mineral. Petrol.* **132**, 34–47.

Strong, H.M. & Tuft, R.E. (1973): The Fe-C system at ~56 kb. *General Electric. Technical Information Series*, Report no 73CRD244, pp. 1-3.

Strunz, H. (1978): *Mineralogische Tabellen*. 7, unveränderte Auflage, Akademische Verlagsgesellschaft Geest & Portig K.-G., Leipzig, 621 SS.

Sugiura, N. (1998): Ion probe measurements of carbon and nitrogen in iron meteorites. *Meteoritics and Planetary Science* **33**, 393–409.

Taylor, W.R. (1990): A reappraisal of the nature of fluids included by diamond - a window to deep-seated mantle fluids and redox conditions. *In:* Stable isotopes and fluid processes in mineralization (H.K. Herbert & S.E. Ho, editors). University of Western Australia, pp. 343-349.

Tsuzuki, A., Sago, S., Hirano, S.I. & Naka, S. (1984): High temperature and pressure preparation and properties of iron carbides Fe_7C_3 and Fe_3C. *J. Materials Science* **19**, 2513–2518.

Ulff-Møller, F. (1985): Solidification history of the Kitdlit lens: Immiscible metal and sulphide liquids from a basaltic dyke on Disko, Central West Greenland. *J. Petrol.* **26**, 64-91.

Weinschenk, E. (1889): Über einige Bestandtheile des Meteoreisens von Magura, Arva, Ungarn. *Annalen des Naturhistorischen Hofmuseums, Wien,* **4**, 93-101.

Win, T.T., Davies, R.M., Griffin, W.L., Wathanakhul, P. & French, D.H. (2001): Distribution and characteristics of diamonds from Myanmar. *J. Asian Earth Sciences* **19**, 563-577.

Wirth, R. (2004): Focused Ion Beam (FIB): A novel technology for advanced application of micro- and nanoanalysis in geosciences and applied mineralogy. *European J. Mineral.* **16**, 863-877.

Wirth, R. (2009): Focused Ion Beam (FIB) combined with SEM and TEM: Advanced analytical tools for studies of chemical composition, microstructure and crystal structure in geomaterials on a nanometre scale. *Chem. Geol.* **261**, 217-229.

Wirth, R., Kaminsky, F., Matsyuk, S. & Schreiber, A. (2009): Unusual micro- and nano-inclusions in diamonds from the Juina area, Brazil. *Earth Planet. Sci. Lett.* **286**, 292-303.

Wood, B. J. (1993): Carbon in the core? *Earth Planet. Sci. Lett.* **117**, 593-607.

Wood, I.G., Vocadlo, L., Knight, K.S., Dobson, D.P., Marshall, W.G., Price, G.D. & Brodholt, J. (2004): Thermal expansion and crystal structure of cementite, Fe_3C, between 4 and 600 K. *J. Appl. Crystallogr.* **37**, 82-90.

Captions to figures

Fig. 1. HAADF image of a part of inclusion in diamond composed of native iron, iron carbide, magnetite, and graphite (Foil #2025). Iron carbide phase is an aggregate of grains, 0.5-1 μm each, having different orientation, which are expressed in various shades of grey in the image. Dark areas in magnetite are pores. Note the high density of dislocations in diamond. The letters A, B and C in the image indicate the locations of the EDX analyses displayed in Fig. 3.

Fig. 2. TEM bright-field image of polycrystalline iron carbide (Foil #2025). Note the high density of dislocations. Some of the dislocation lines are straight, indicating dislocation glide; many of them are curved and bent indicating a diffusion-controlled deformation mechanism.

Fig. 3. EDX spectra of minerals comprising the inclusion (Foil #2025) . A – Iron carbide with admixture of nitrogen. B – Native iron with admixture of nitrogen. C – Magnetite. Copper peaks are artefacts caused by the copper grid; and Ga peaks are caused by the implanted Ga-ions from

the focused ion beam (FIB) technique during foil-milling. The carbon signal comes from the underlying carbon film.

Fig. 4. Indexed electron diffraction patterns (FFT) from HREM images of iron carbide grains. A - Fe_2C crystal in foil #2025 with the zone axis [00-1]. B – Fe_3C crystal in foil #2053 with the zone axis [-101]. C - Fe_2C crystal in foil #2053 with the zone axis of [00-1]. Note weak additional spots between (h00) reflections and (010) and (210) reflections, which can be indexed as (100) and (110) reflections. D – Iron carbonitride in foil # 2053 with the zone axis [010]

Fig. 5. HAADF image of a graphite – iron carbide inclusion in diamond (Foil #2049). Iron carbide is developed along the interface with diamond and as finely-dispersed bright spots in the graphite matrix.

Fig. 6. TEM images of a plate-like inclusion in diamond, composed of iron carbide in a graphite matrix (Foil #2053). A – Bright field (BF) image. The dark rounded shadow is due to the perforated carbon film onto which the TEM foil rests. B – Dark field (DF) image. The bright areas represent iron carbide crystals with the same crystallographic orientation.

Fig. 7. TEM bright-field image showing a section of the plate-like inclusion in diamond (Foil #2053). Note the even interface between iron carbide and diamond, whereas the interface between iron carbide and graphite is always irregular. Small iron carbide fragments of an originally larger grain are present in the graphite matrix.

Fig. 8. TEM bright-field image of iron carbide platelets in a plate-like inclusion in diamond (Foil #2063). The strong dark diffraction contrast of the iron carbide platelets is due to similar orientation of the individual platelets, oriented with a low indexed zone axis parallel to the optical axis.

Fig. 9. High-resolution TEM image of an iron carbide platelet tip in foil #2063. The tip is coated with a thin (*ca*. 5-6 nm) graphite layer. Lattice fringes of (0002) graphite displayed in the image have a spacing of 0.335 nm. The assemblage of iron carbide with the well-crystallized graphite layer is embedded in poorly crystallized graphite or amorphous carbon.

Fig. 10. HAADF image of an iron carbide - graphite inclusion in diamond (Foil #2073).

Fig. 11. EEL spectrum of "chalypite" from foil #2053. Note the presence of the nitrogen N-*K* edge.

Fig. 12. Histogram of Fe/C distribution in grains of iron carbide from sample #8/1-03. Black dots show Fe/C values for individual analyses in Table 3.

Fig. 13. The Fe-rich portion of the Fe–C phase diagram at 50 and 130 GPa (after Lord *et al.*, 2009). L, liquid; Di, diamond. Values in italics represent melting temperatures and those in bold represent compositions.

Titles for tables

Table 1. Diffraction data for iron carbide grains.

Table 2. Chemical compositions of iron carbide grains from foil #2053 (at.%, EELS data).

Table 3. Composition of metals in magnetite and iron carbides (at.%, AEM and EELS data).

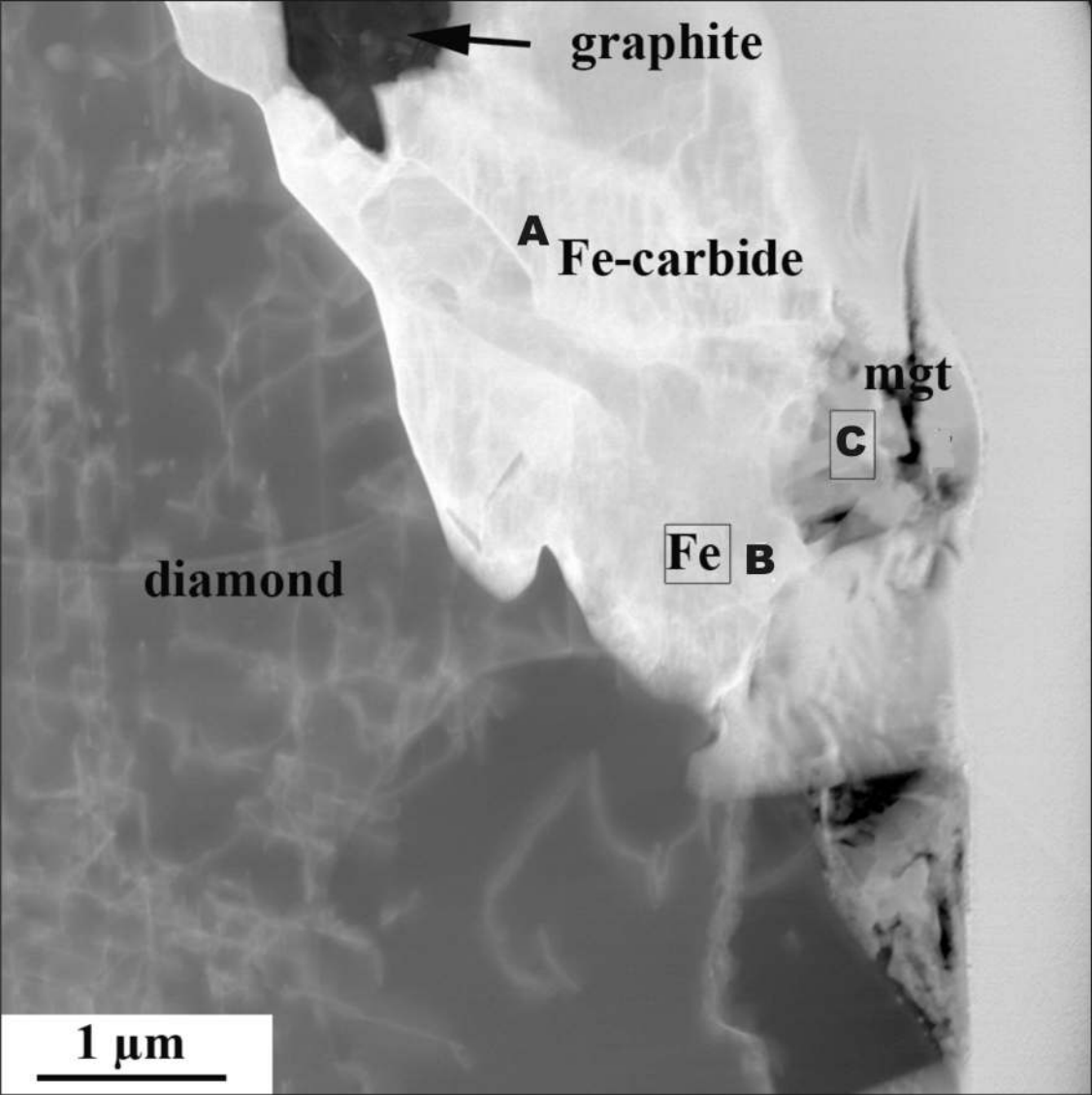
graphite
A
Fe-carbide
mgt
C
Fe
B
diamond
1 µm

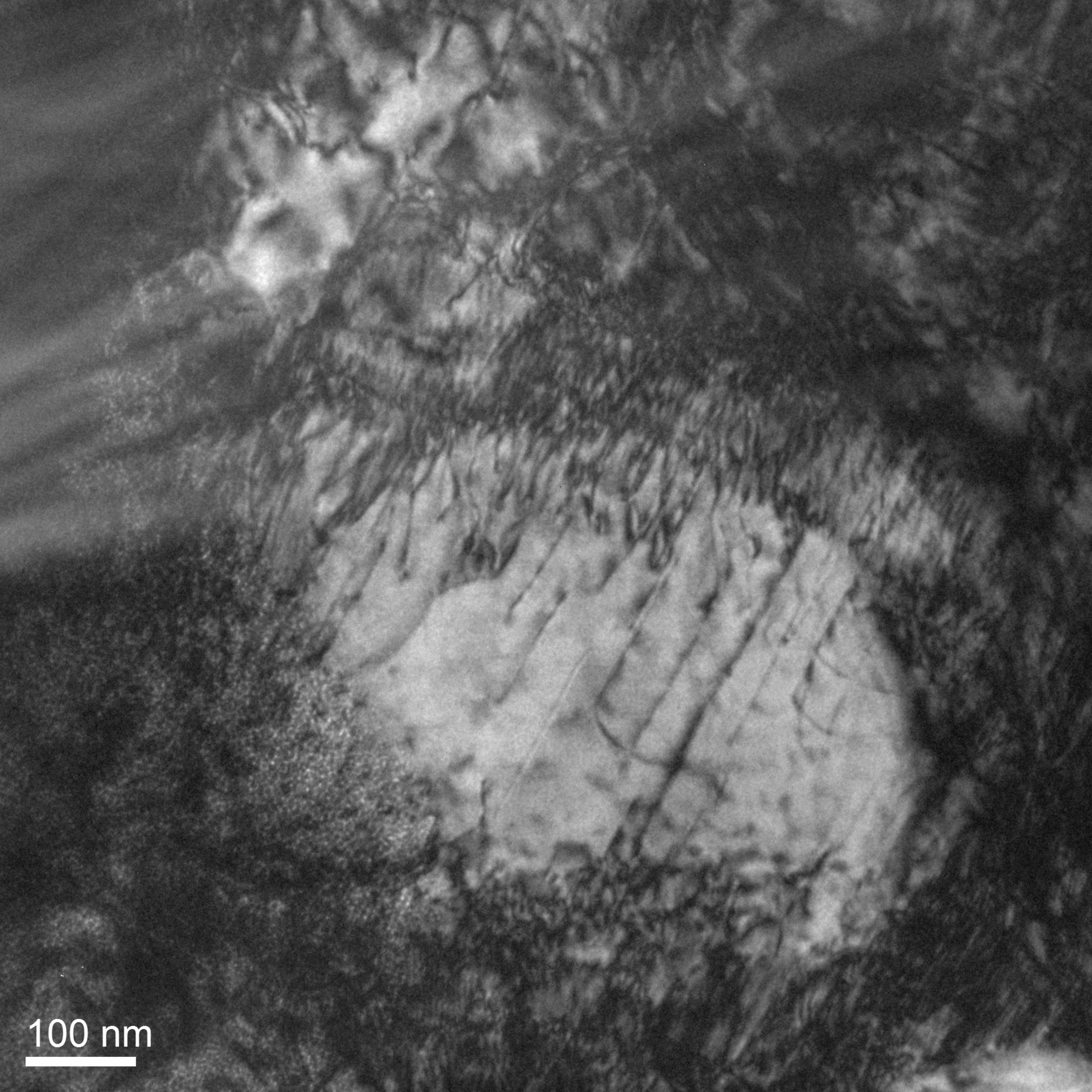
100 nm

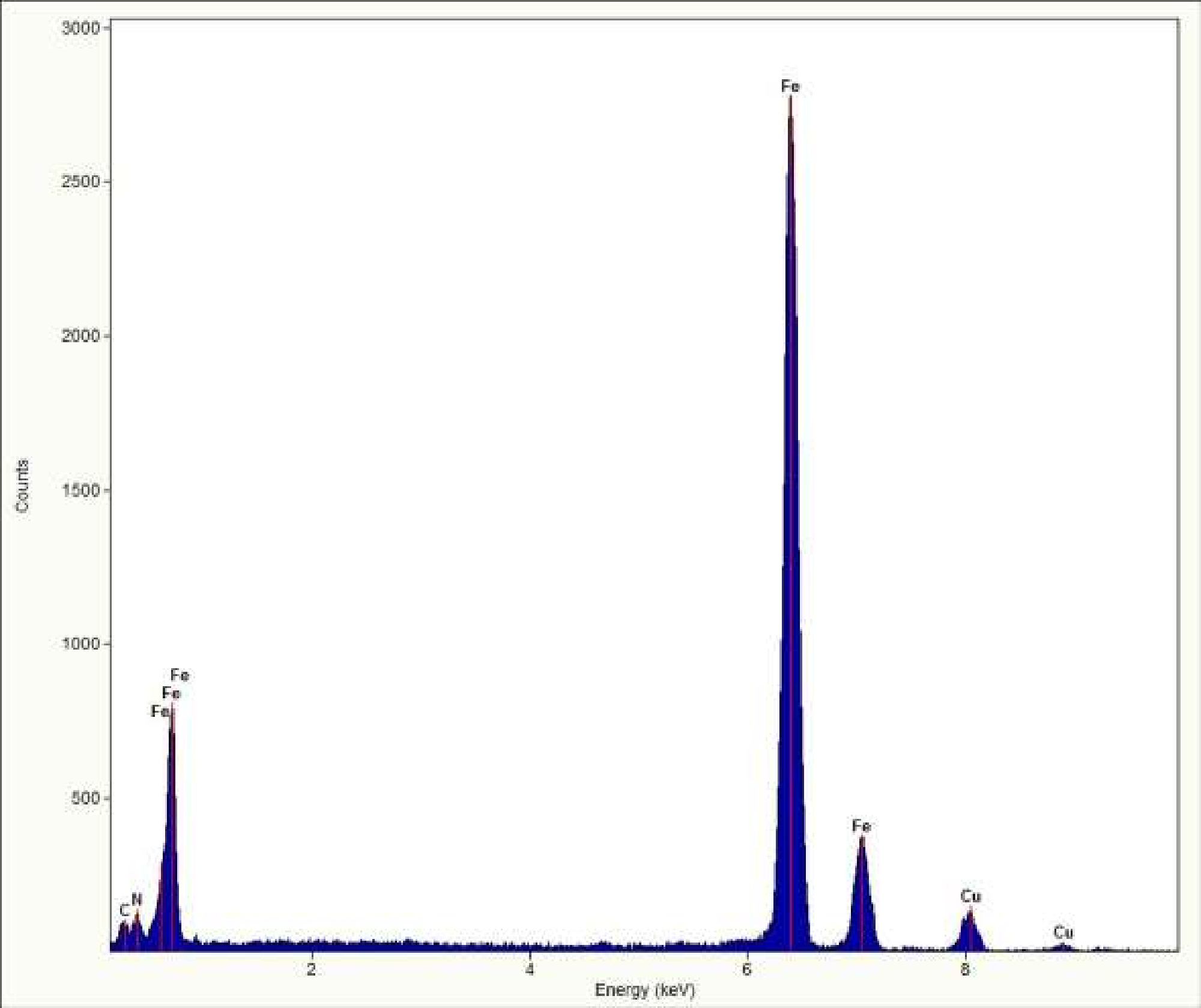
3000
2500
2000
1500
1000
500
Counts
Fe
Fe
Fe
Fe
Fe
C
N
Fe
Cu
Cu
2
4
6
8
Energy (keV)

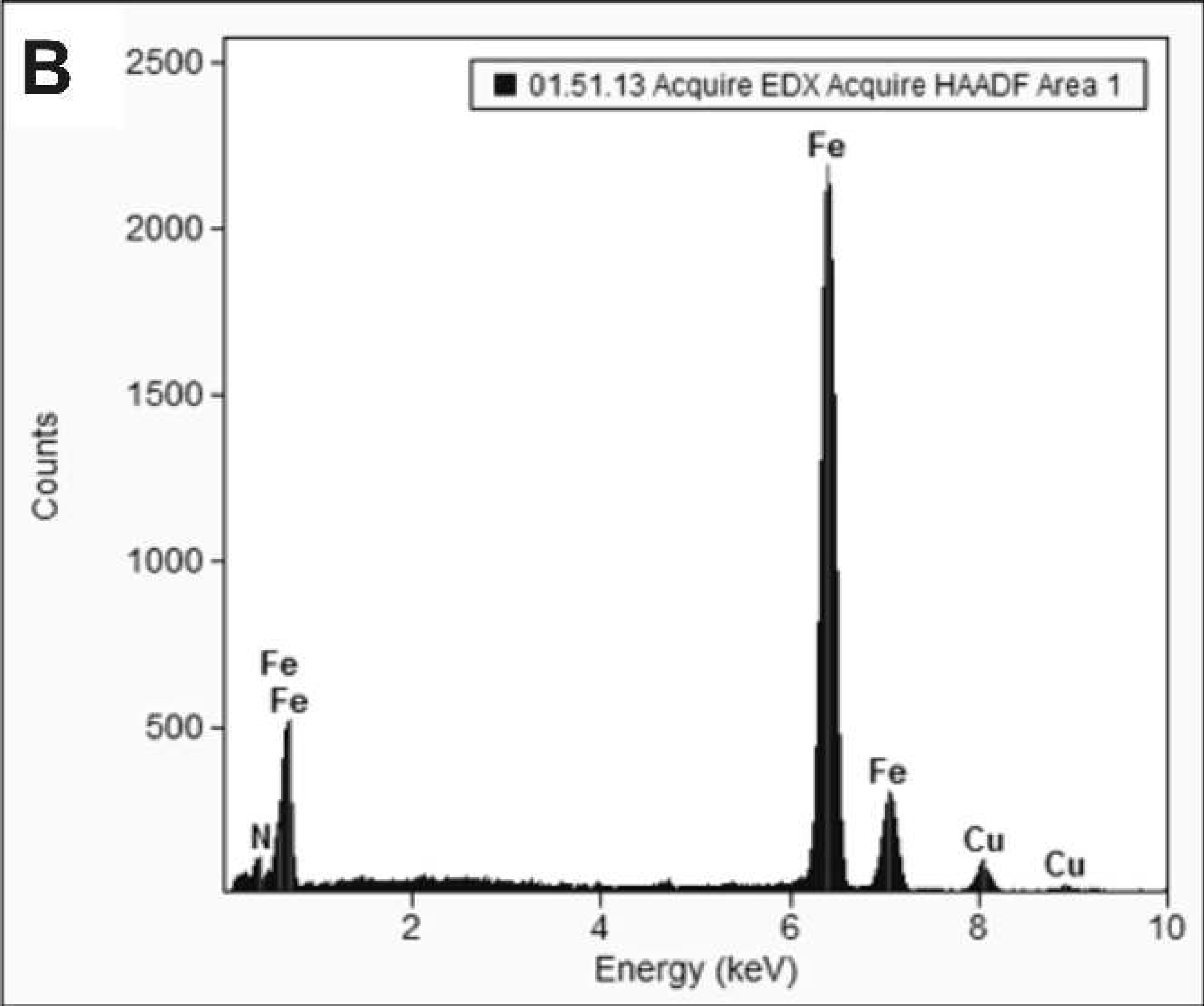
B
01.51.13 Acquire EDX Acquire HAADF Area 1
Counts
2500
2000
1500
1000
500
Fe
Fe
Fe
N
Fe
Cu
Cu
2
4
6
8
10
Energy (keV)

C

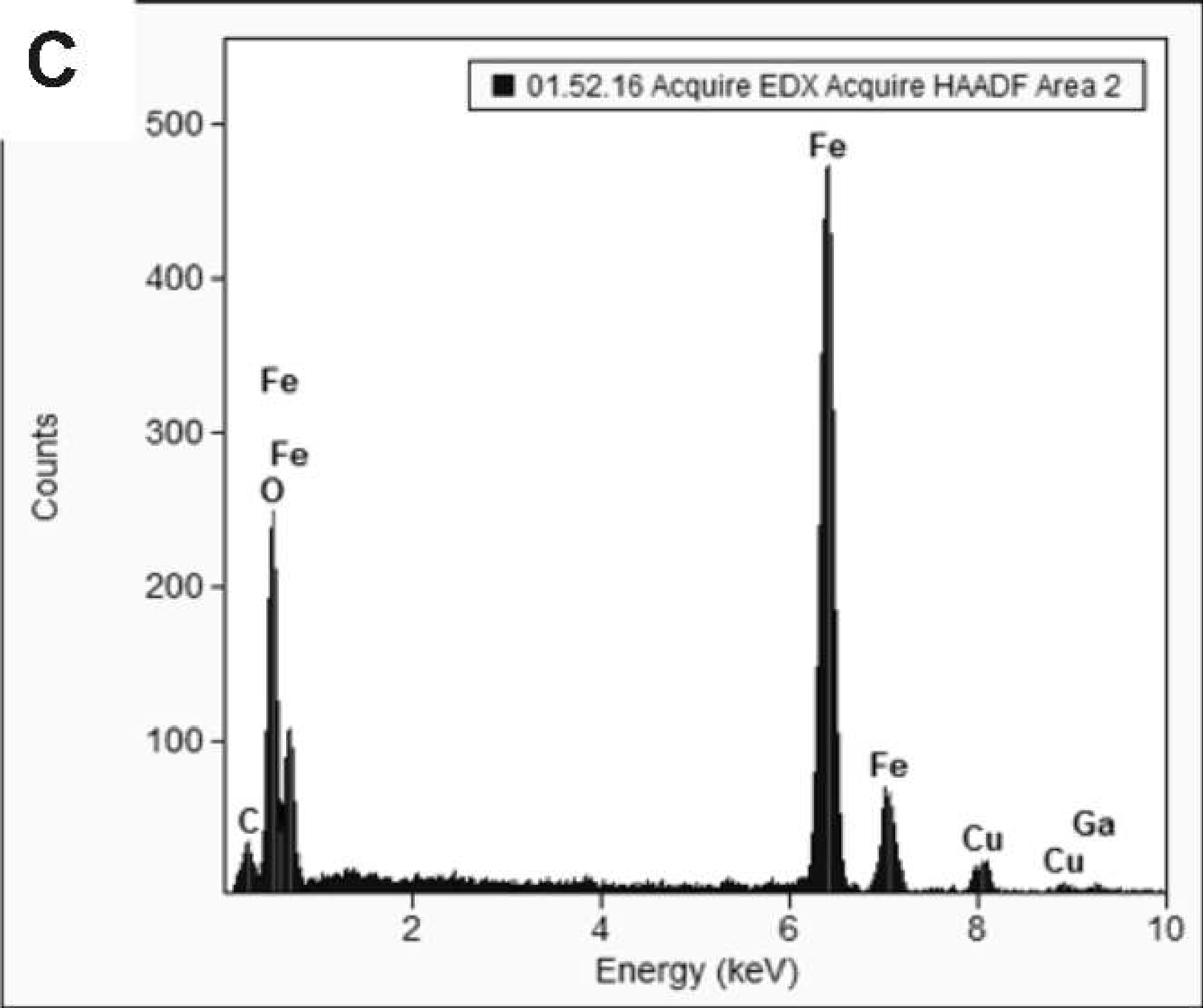
01.52.16 Acquire EDX Acquire HAADF Area 2
Counts
500
400
300
200
100
Fe
Fe
O
C
Fe
Fe
Cu
Cu
Ga
2
4
6
8
10
Energy (keV)

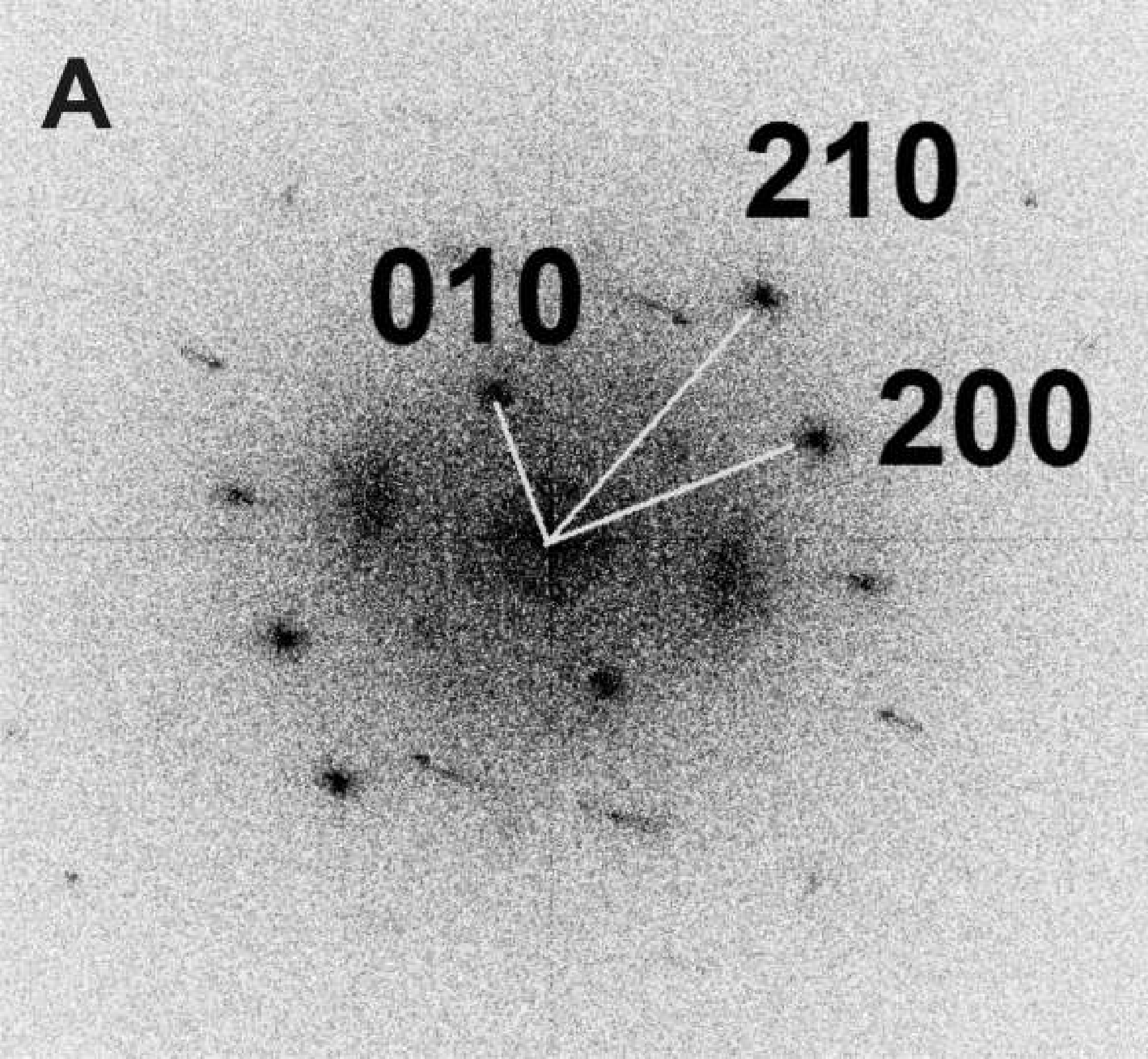
A
210
010
200

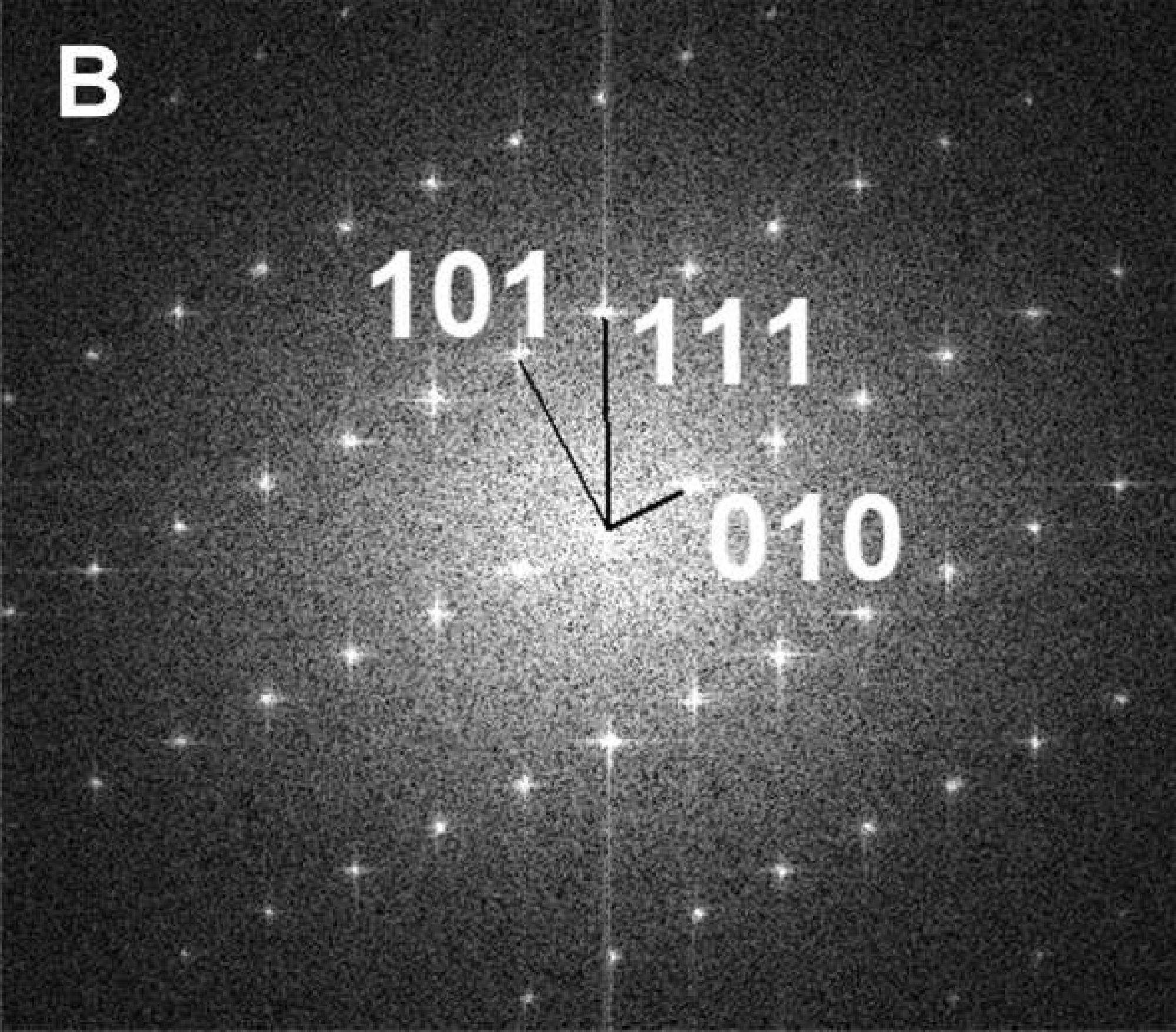
B
101
111
010

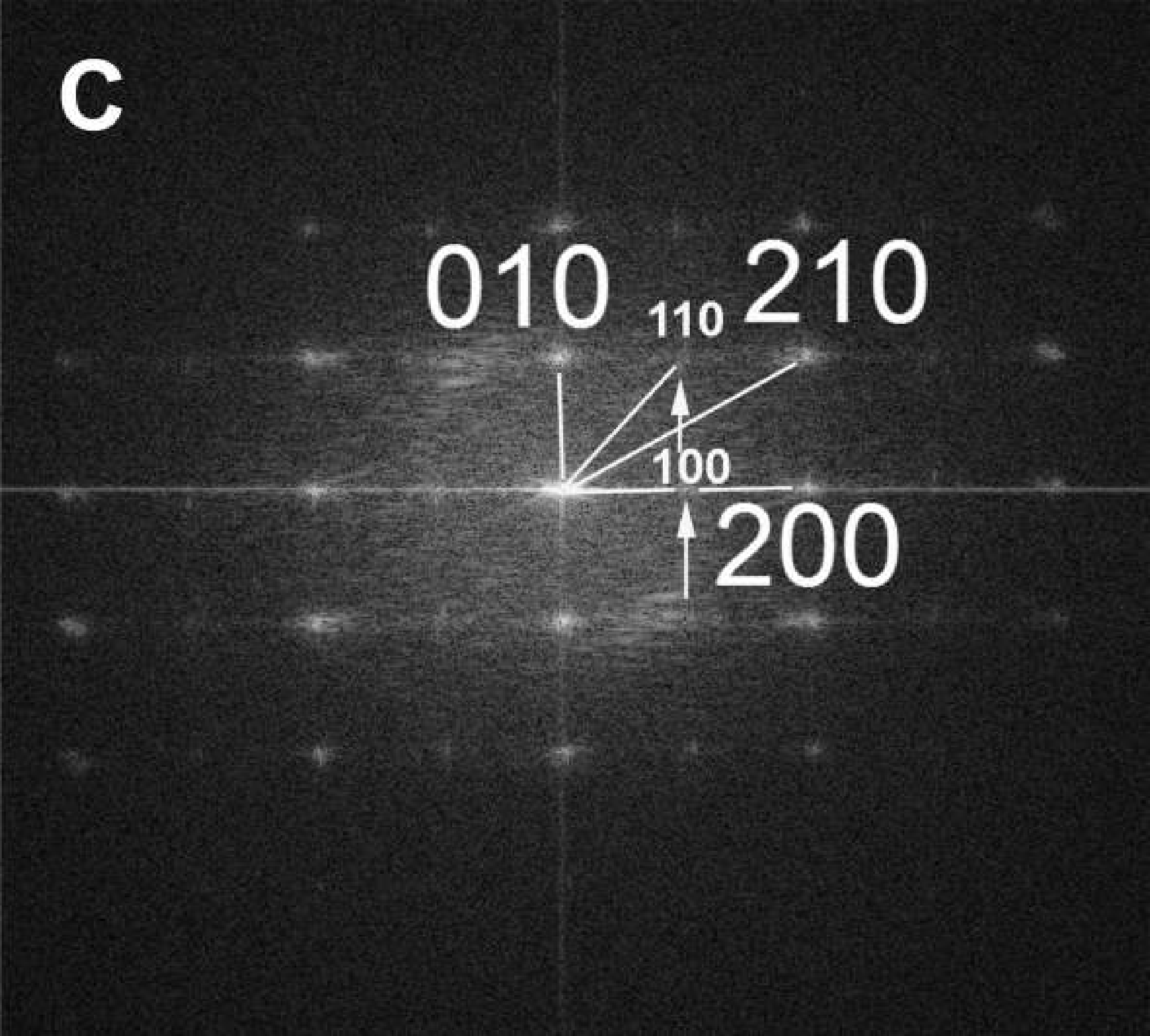
C
010
110
210
100
200

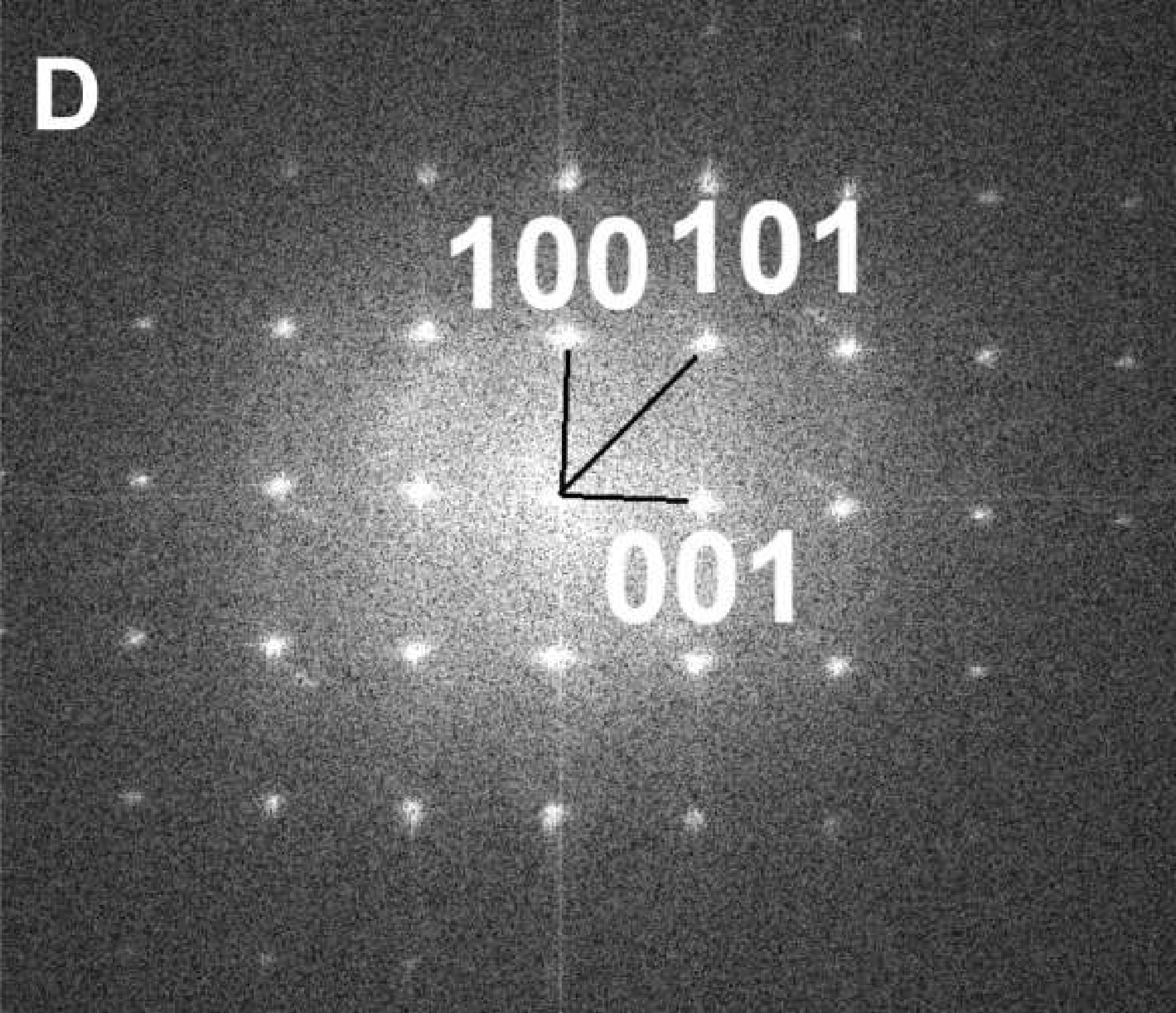
D
100 101
001

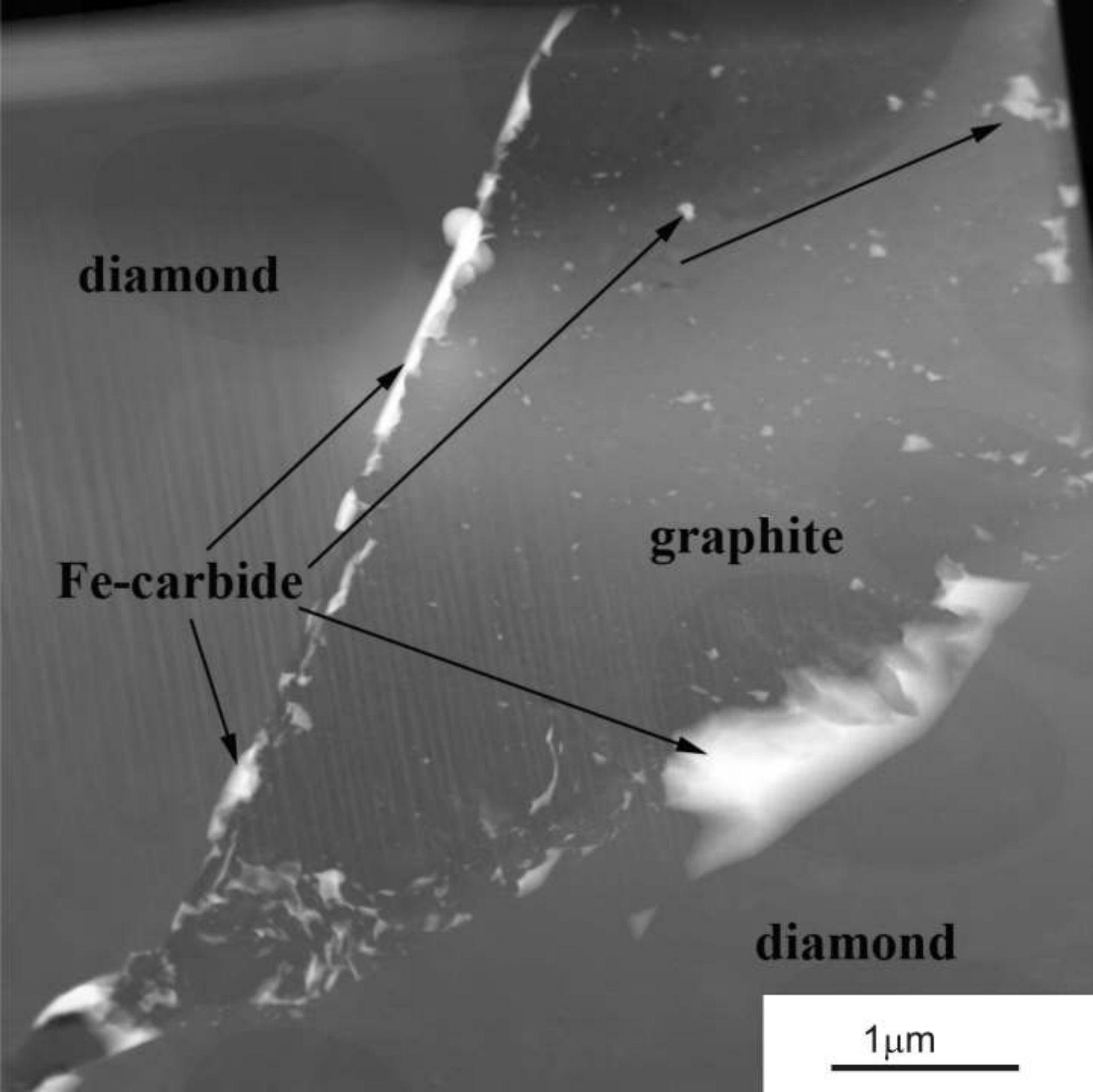
diamond
graphite
Fe-carbide
diamond
1μm

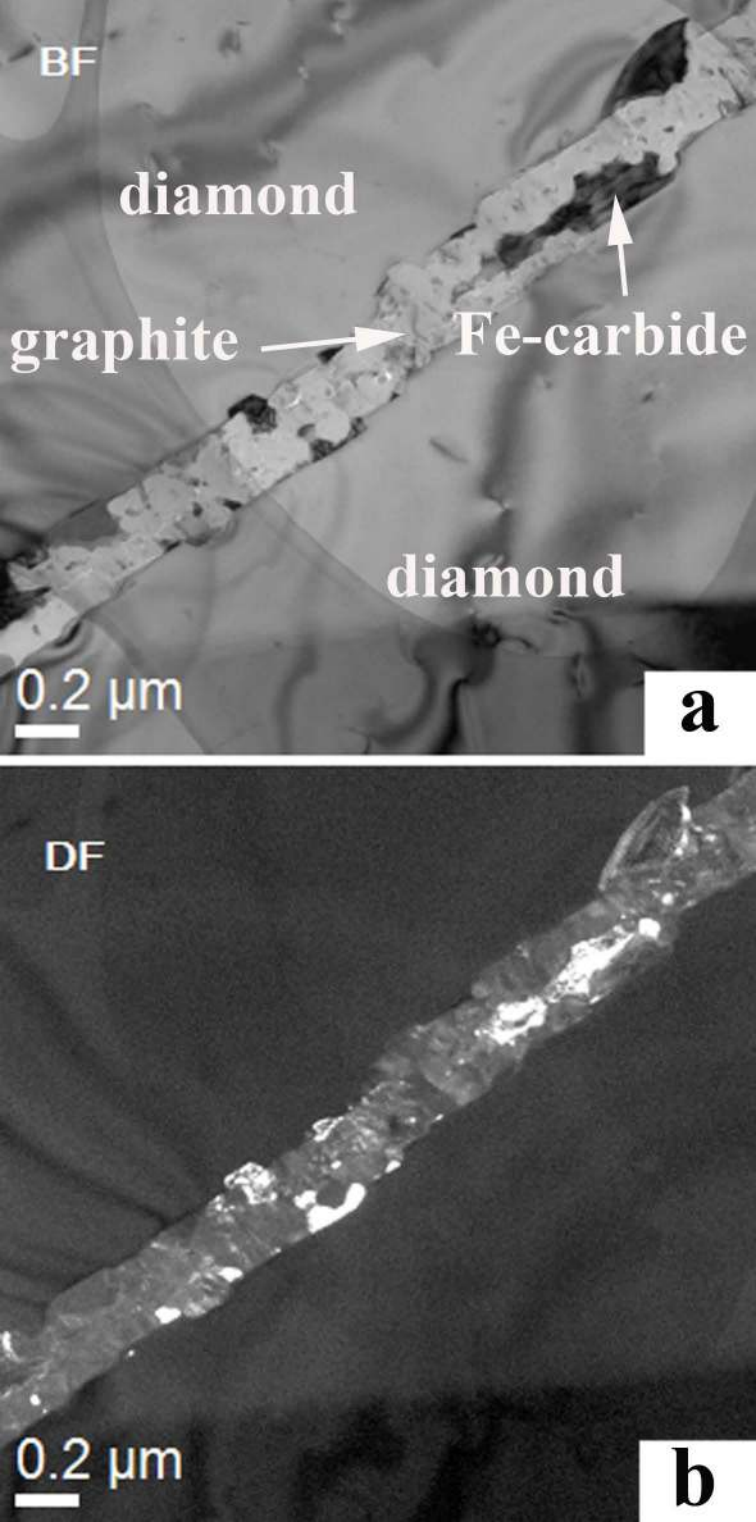
BF
diamond
graphite
Fe-carbide
diamond
0.2 μm
a
DF
0.2 μm
b

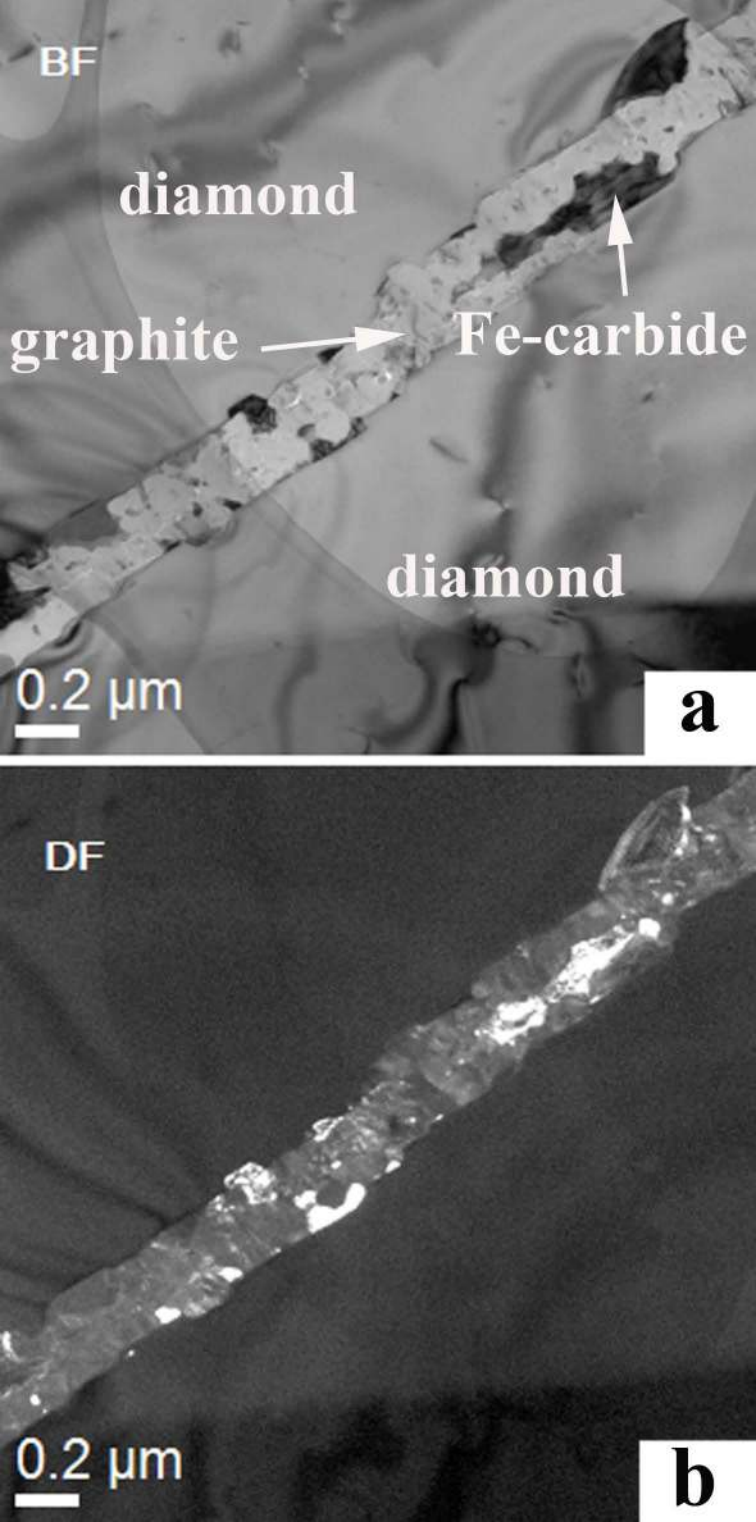
BF
diamond
graphite
Fe-carbide
diamond
0.2 μm
a
DF
0.2 μm
b

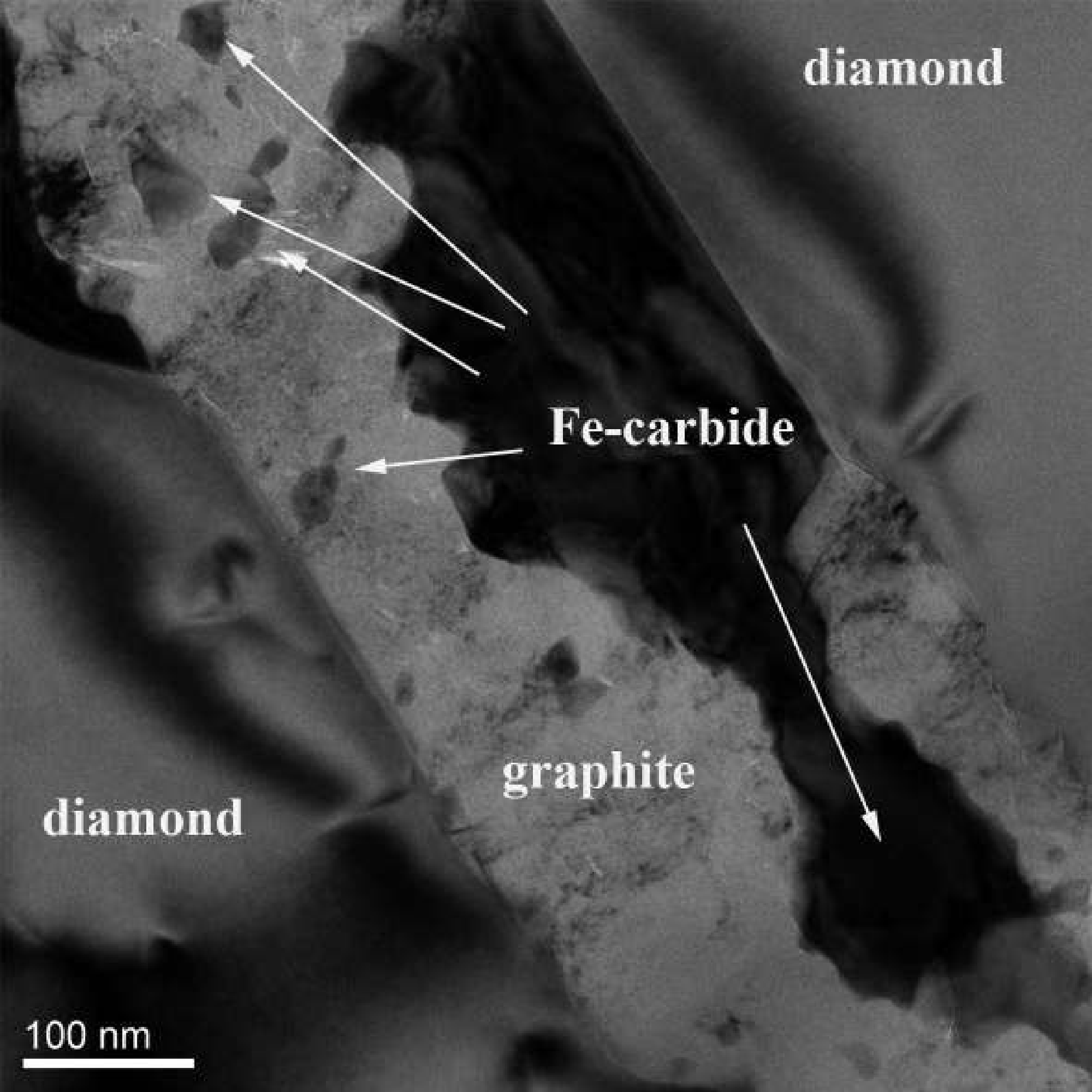
diamond
Fe-carbide
graphite
diamond
100 nm

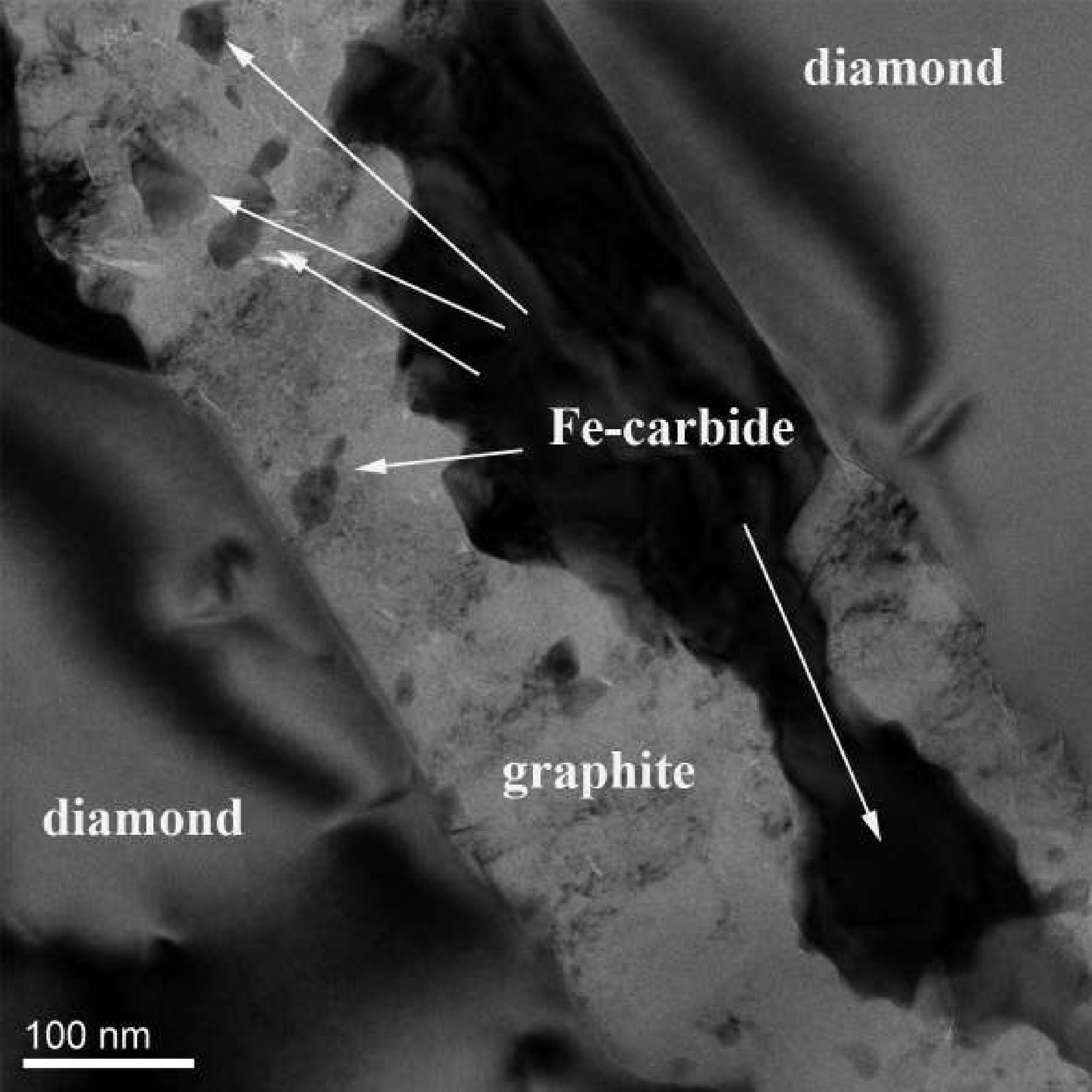
diamond
Fe-carbide
graphite
diamond
100 nm

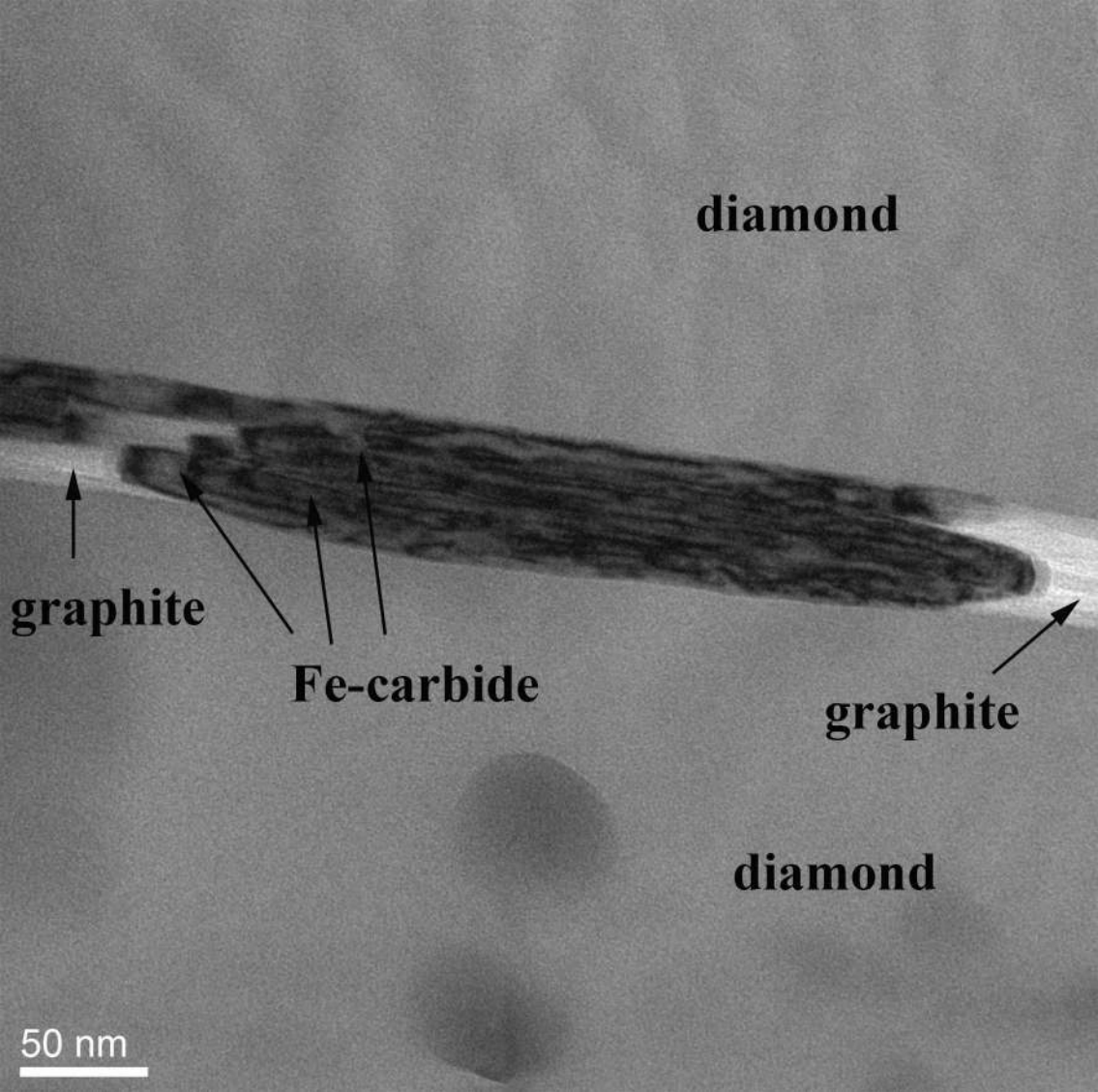
diamond
graphite
Fe-carbide
graphite
diamond
50 nm

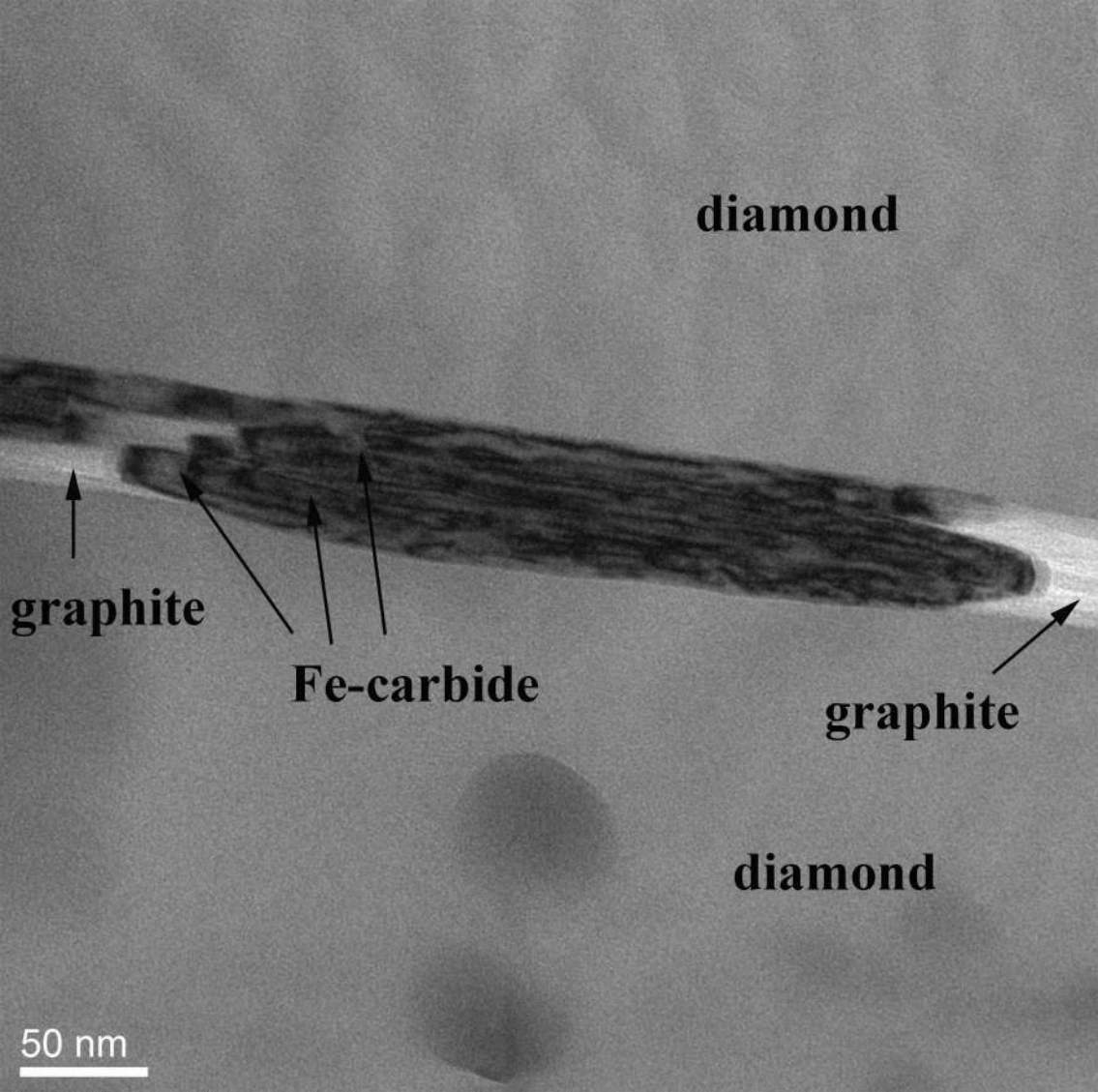
diamond
graphite
Fe-carbide
graphite
diamond
50 nm

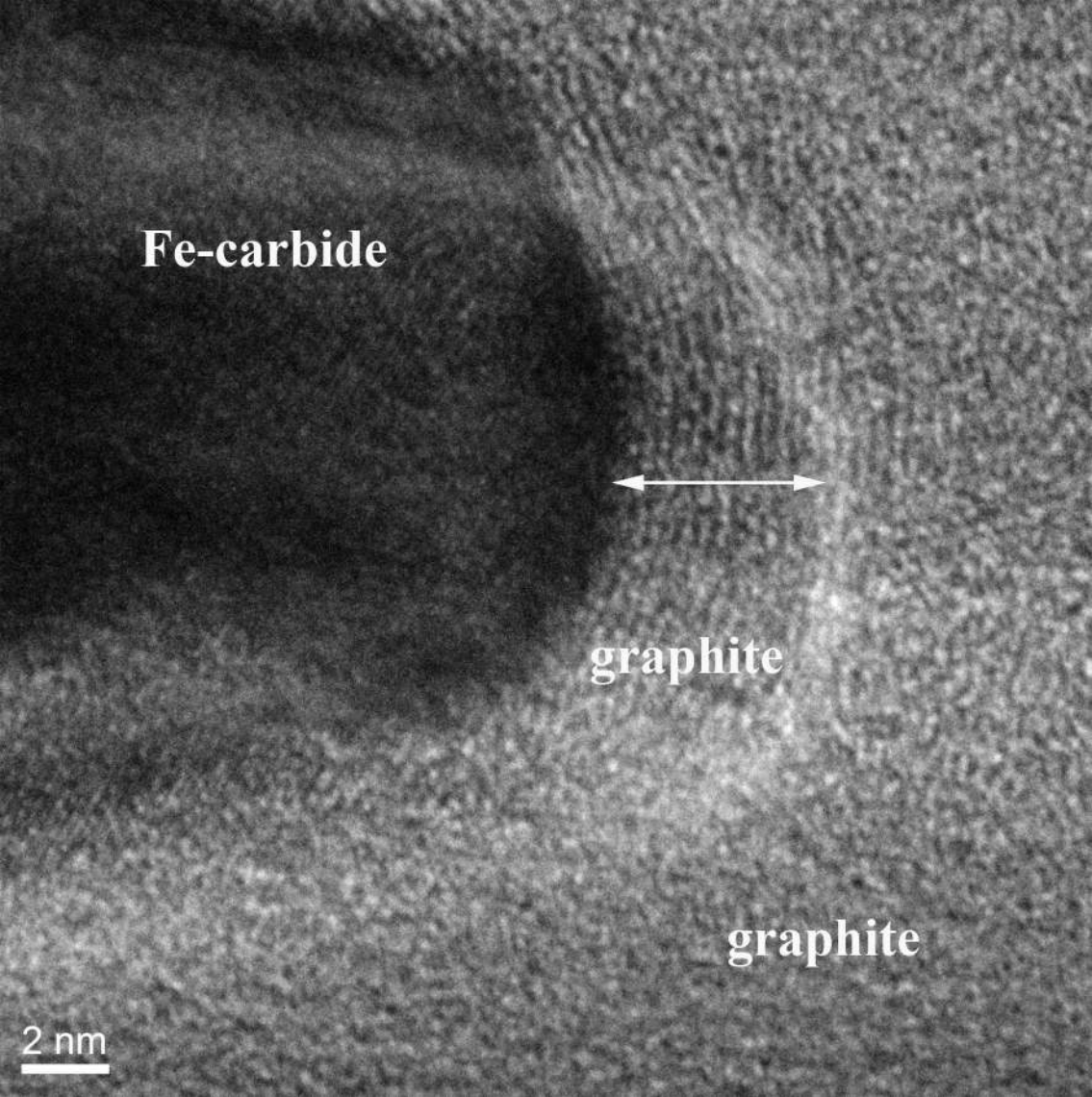
Fe-carbide
graphite
graphite
2 nm

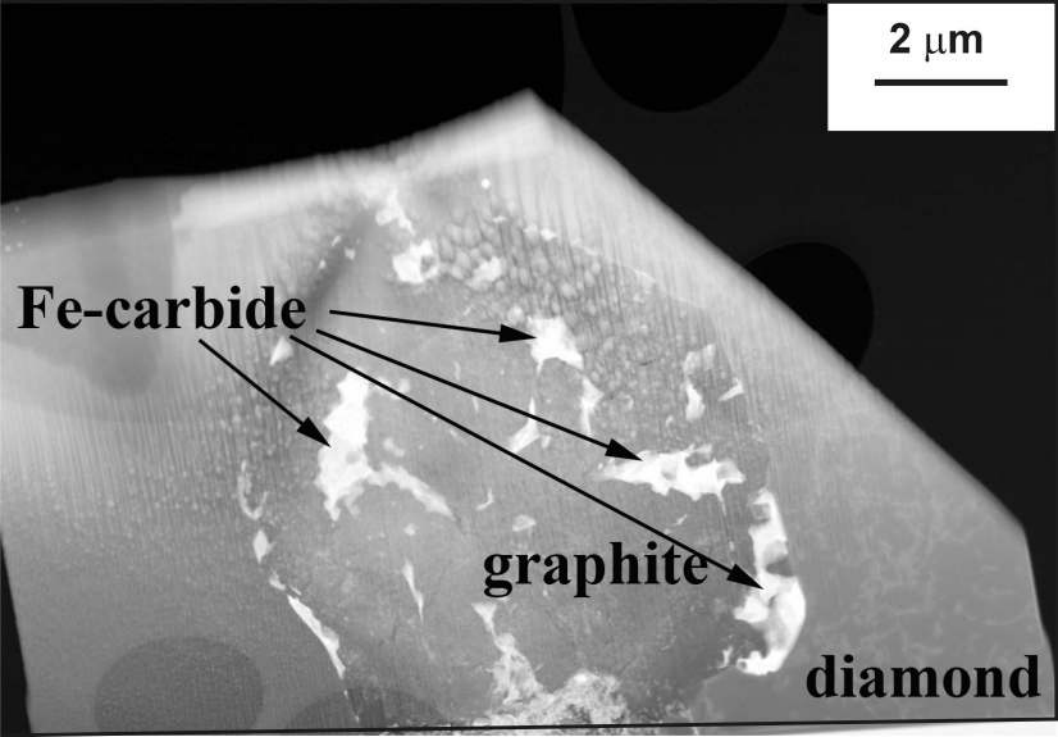
2 μm
Fe-carbide
graphite
diamond

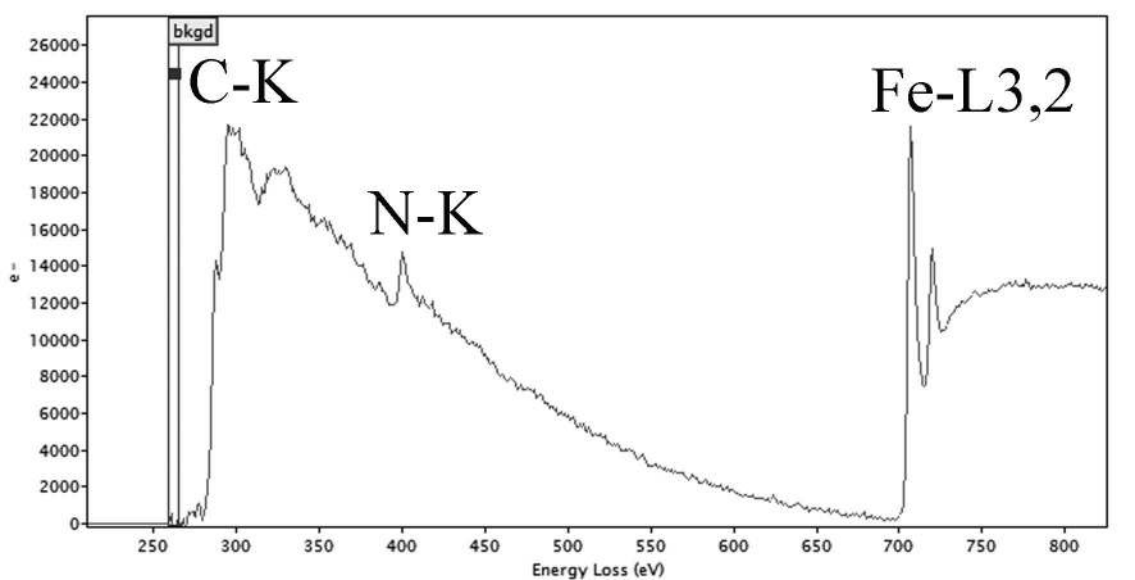
bkgd
C-K
N-K
Fe-L3,2
e⁻
Energy Loss (eV)
0
2000
4000
6000
8000
10000
12000
14000
16000
18000
20000
22000
24000
26000
250
300
350
400
450
500
550
600
650
700
750
800

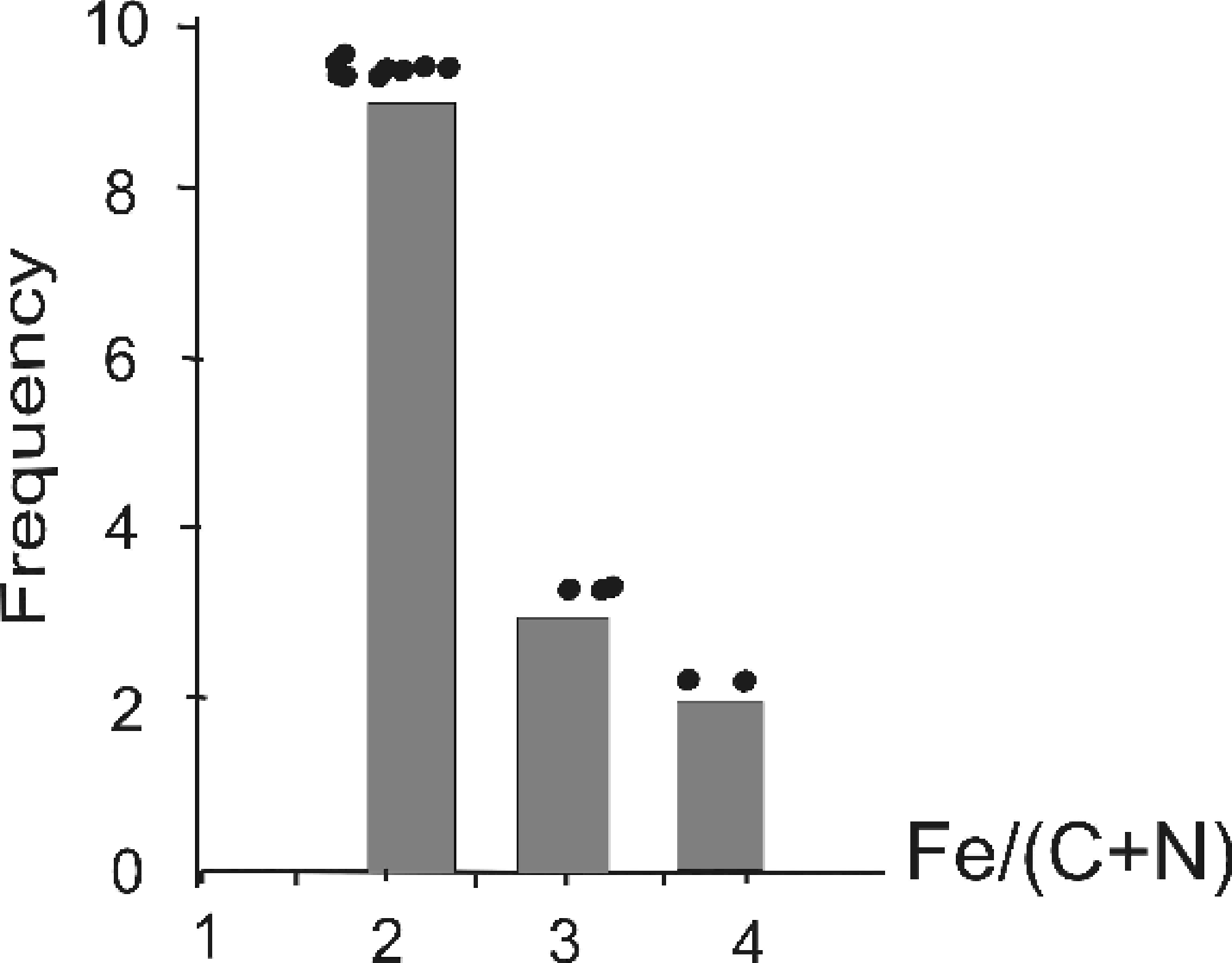
Frequency
10
8
6
4
2
0
1
2
3
4
Fe/(C+N)

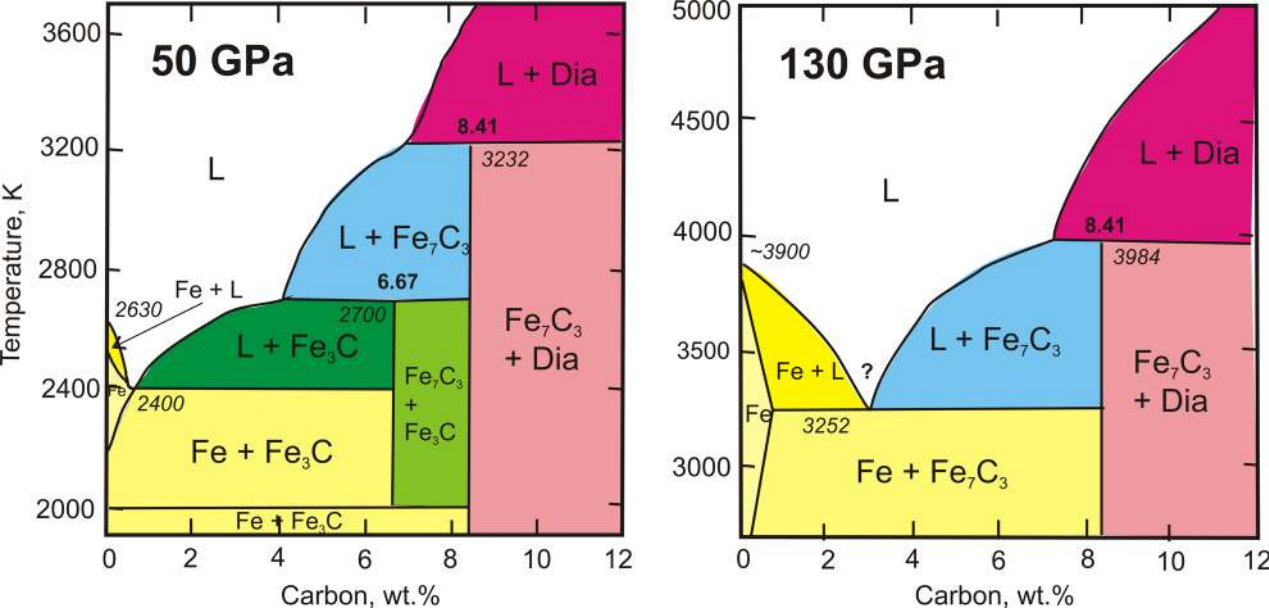
50 GPa
L + Dia
8.41
L
3232
L + Fe7C3
6.67
Fe + L
2630
2700
L + Fe3C
Fe7C3
+ Dia
Fe7C3
+
Fe3C
2400
Fe + Fe3C
Fe + Fe3C
Temperature, K
Carbon, wt.%
130 GPa
L + Dia
L
8.41
~3900
3984
L + Fe7C3
Fe + L
?
Fe
3252
Fe7C3
+ Dia
Fe + Fe7C3
Carbon, wt.%

Table 1. Diffraction data for iron carbide grains.

Cohenite				Chalypite				Carbonitride		
	Calculated	Observed			Calculated	Observed			Calculated	Observed
Indices	Fe_3C from Fruchart *et al.*, 1984	Foil #2025	Foil #2053*	Indices	Fe_2C from Hirotsu & Nagakura, 1972	Foil #2025**	Foil #2053***	Indices	$Fe_3(N,C)_{1.395}$ from Leineweber *et al.*, 2001	Foil #2053****
	1	2	3	4	5	6	7	8	9	10
	d_{hkl} (nm)				d_{hkl} (nm)				d_{hkl} (nm)	
(100)	0.509			(100)	0.4704		0.464			
(010)	0.6748		0.675	(010)	0.4318	0.426	0.434			
(001)	0.4523	0.43		(001)	0.2830			(001)	0.4406	0.447
(011)	0.3757			(110)	0.3181		0.321	(100)	0.4135	0.402
(101)	0.3381		0.337	(101)	0.2425			(101)	0.3015	0.299
(111)	0.3023		0.299	(011)	0.2367	0.237				
(200)	0.2545			(200)	0.2352		0.232			
(121)	0.2388	0.237		(111)	0.2114	0.21				
(210)	0.2381	0.237		(210)	0.2065	0.21	0.204			
(002)	0.2261			(211)	0.1668					
(201)	0.2218									
(211)	0.2107	0.21								
Zone axis		[1-20]	[-101]			[00-1]	[00-1]			[010]
	Angles between planes, degrees				Angles between planes, degrees				Angles between planes, degrees	
(001):(211)	62.23	63.0		(010):(210)	61.4	61.9	61.8			
(211):210)	27.77	28.0		(200):(210)	28.58	27.8	28.4			
(010):(111)	63.39		63.8					(101):(001)	46.82	47.8
(101):(111)	26.61		26.7					(101):(100)	43.18	42.5

Note: * See diffractogram in Fig. 4B; chemical composition in Table 2, grain #11.

** See diffractogram in Fig. 4A.

*** See diffractogram in Fig. 4C; chemical composition in Table 2, grain #12.

**** See diffractogram in Fig. 4D.

Table 2. Chemical compositions of iron carbide grains from foil #2053 (at.%, EELS data).

Grain #	Fe	C	N	Fe/(C+N)	C/(C+N)	Note
1	68.2	31.8	n/a	2.14	-	
2	67.4	32.6	n/a	2.07	-	
3	78.2	21.8	n/a	3.59	-	
4	75.1	24.9	n/a	3.02	-	
5	66.5	33.5	n/a	1.99	-	
6	79.9	20.1	n/a	3.98	-	
7	66.1	33.9	n/a	1.95	-	
8	77.2	22.8	n/a	3.39	-	
9	62.2	37.8	n/a	1.65	-	Two points in the same grain
	62.4	37.6	n/a	1.66	-	
10	62.2	37.8	n/a	1.65	-	Profile across the grain
	66.2	33.8	n/a	1.96	-	Profile across the grain
	63.7	36.3	n/a	1.75	-	Profile across the grain
	63.5	36.5	n/a	1.74	-	Profile across the grain
10 av.	63.9	36.1	n/a	1.77	-	Average of 4 (σ = 0.11)
11	76.9	23.1	bdl	3.33	-	Anal. #3 in Table 1
12	62.8	28.1	9.1	1.69	0.76	Anal. #7 in Table 1
13	62.2	30.5	7.3	1.65	0.81	Other grains with the same orientation as #12
14	69.9	22.1	8.0	2.32	0.73	

Note: n/a – not analyzed; bdl – below detection limit.

Table 3. Composition of metals in magnetite and iron carbides (at.%, AEM and EELS data).

Foil #	Mineral	Fe	Cr	Ni
2025	Magnetite	99.72	0.28	-
	Magnetite	99.72	0.28	-
	Iron carbide	99.74	-	0.26
	Iron carbide	99.74	0.03	0.23
2049	Iron carbide	100.00	-	-
	Iron carbide	99.87	0.05	0.08
	Iron carbide	99.84	0.06	0.10
2063	Iron carbide	100.00	-	-
	Iron carbide	100.00	-	-
	Iron carbide	100.00	-	-
2073	Iron carbide	98.20	1.30	0.50